

Multi-source adversarial transfer learning for ultrasound image segmentation with limited similarity

Yifu Zhang^a, Hongru Li^{a,*}, Tao Yang^a, Rui Tao^a, Zhengyuan Liu^b, Shimeng Shi^a, Jiansong Zhang^c, Ning Ma^a, Wujin Feng^a, Zhanhu Zhang^a, Xinyu Zhang^a

^a*College of Information Sciences and Engineering, Northeastern University, Shenyang, 110819, China*

^b*Schwarzman College, Tsinghua University, Beijing, 100084, China*

^c*Henan Education Technology Equipment Management Center, Zhengzhou 450004, China*

Abstract

Lesion segmentation of ultrasound medical images based on deep learning techniques is a widely used method for diagnosing diseases. Although there is a large amount of ultrasound image data in medical centers and other places, labeled ultrasound datasets are a scarce resource, and it is likely that no datasets are available for new tissues/organs. Transfer learning provides the possibility to solve this problem, but there are too many features in natural images that are not related to the target domain. As a source domain, redundant features that are not conducive to the task will be extracted. Migration between ultrasound images can avoid this problem, but there are few types of public datasets, and it is difficult to find sufficiently similar source domains. Compared with natural images, ultrasound images have less information, and there are fewer transferable features between different ultrasound images, which may cause negative transfer. To this end, a multi-source adversarial transfer learning network for ultrasound image segmentation is proposed. Specifically, to address the lack of annotations, the idea of adversarial transfer learning is used to adaptively extract common features between a certain pair of source and target domains,

*Correspondence to: College of Information Sciences and Engineering, Northeastern University, NO. 3-11, Wenhua Road, Heping District, Shenyang, 110819, China.

Email addresses: 2000912@stu.neu.edu.cn (Yifu Zhang), lihongru@ise.neu.edu.cn (Hongru Li)

which provides the possibility to utilize unlabeled ultrasound data. To alleviate the lack of knowledge in a single source domain, multi-source transfer learning is adopted to fuse knowledge from multiple source domains. In order to ensure the effectiveness of the fusion and maximize the use of precious data, a multi-source domain independent strategy is also proposed to improve the estimation of the target domain data distribution, which further increases the learning ability of the multi-source adversarial migration learning network in multiple domains. The effectiveness of multi-source adversarial transfer learning is demonstrated through experiments on three datasets of ultrasound image datasets.

Keywords: Ultrasound medical image segmentation, Deep learning, Multi-Source Adversarial Transfer Learning, U-Net

1. INTRODUCTION

With the development of artificial intelligence, medical image diagnosis plays an increasingly important role[1]. Due to the advantages of high efficiency, non-invasiveness, non-radiation, and no need to inject contrast agents that are harmful to the human body, ultrasound medical image segmentation[2] has become a representative method. However, ultrasound images have low contrast and small signal-to-noise ratio, due to the blurred boundary between segmentation target and background and the inherent characteristics of a large number of echo disturbances, speckle noise and acoustic shadows[3, 4, 5], this results in the traditional segmentation method [6] being less effective.

Deep learning [7] represented by the U-Net network[10] has the potential to automatically perform ultrasound image analysis tasks[8, 9]. It has been used in the occasions such as breast ultrasound image segmentation [11], coronary artery ultrasound image segmentation [12]. However, the high cost of labeling results in ultrasound image datasets generally having a small sample size, and deep networks can easily lead to overfitting[13] problems when learning directly from such datasets.

Transfer learning provides a potential approach [15] for the problem of insuf-

ficient annotation data, because there are always some similar parts [16] in things in nature. It has been applied in life expectancy[17, 18], vehicle driving behavior recognition[19], advertising fraud detection[20], EEG pattern recognition[21] and other fields. Transfer learning makes it important to leverage medical resources from different sources [14], For example, Yap et al. [22] used transfer learning FCN-AlexNet to detect breast cancer ultrasound images, and achieved good results; In the literature[23], the transfer of natural images to ultrasound images is called cross-domain transfer, and the transfer between different medical images (such as between ultrasound images, between CT and ultrasound images) is called cross-modal transfer[24]. The cross-modal transfer is easier to achieve better results than the cross-domain transfer because there are too many features in natural images that are not related to the target domain, which will lead to the extraction of redundant features that are not conducive to the task. Song et al.[25] used different imaging methods of the same organ for transfer learning. They used a large amount of labeled CT modal data to solve the problem of the lack of ultrasound training data with cross-modal transfer learning. To mitigate the huge domain difference between ultrasound and CT, they employ CycleGAN[26] to synthesize ultrasound images from CT data to construct a transition dataset [27] for pre-training. Additionally, radiologists often use previously acquired knowledge from ultrasound images of one tissue/organ type to enhance the interpretation of another type of image. For example, calcifications have a similar appearance in ultrasound breast images and ultrasound tendon images, which helps radiologists with ultrasound breast experience quickly learn to interpret calcified tendon images. Huang et al.[28] were inspired to try cross-modal transfer of ultrasound images between similar tissues and organs. However, the efficiency of transfer strongly depends on the similarity between the source and target tasks, as their dissimilarity is a major contributor to negative transfer [29]. Moreover, due to ethical and other issues, there are few types of open-access ultrasound datasets, and it is difficult to obtain source-domain ultrasound datasets that are sufficiently similar to the target domain. In addition, the boundary between the target to be

segmented (such as pathological tissue) and the background (such as normal tissue) in medical images such as ultrasound is blurred and similar in texture. It is very difficult to accurately extract visual representations and improve semantic transferability[30, 31]. Therefore, it is of great significance to extract as much knowledge as possible between ultrasound source domain and target domain with different sources and limited similarity.

In addition to using different sources of labeled data, the unlabeled target domain data is also of great significance. Recently, adversarial thinking has been widely used to adaptively extract domain-invariant features, resulting in a method called adversarial transfer learning[32, 33]. This method of evaluating the generality of deep features based on the output of the domain classifier can implicitly design a metric function, so it can avoid the designer’s experience limitation and adaptively extract common deep features between domains. In industry, it has been applied in life prediction[34], SLAM positioning[35], fault diagnosis, etc.[36]; In terms of medical image segmentation, which has been applied to whole-heart segmentation[37], optic disc segmentation[38], mitochondrial segmentation[39], retinal anomaly segmentation[40] and transmembrane liver segmentation[41],etc. However, to obtain enough key features in adversarial transfer learning, the source and target domains need to have sufficient similarity. The literature [42] points out that the properties of different domains can vary widely, especially in the medical field, where the data are heterogeneous, because its source (eg, different patients, sensors, collection environment), different formats (eg, image resolution, sampling frequency), different scales (eg, color scale of images, units of physical or physiological measurement), or just have different probability distributions in different quantities. Moreover, there are certain differences in the images of various organs of the human body. In addition, there are currently fewer types of source domains that are publicly available for selection. When faced with a certain target domain disease it may not even be possible to find a sufficiently similar source domain.

Although a single source domain and target domain are not sufficiently similar, there are always similarities between different types of ultrasound images,

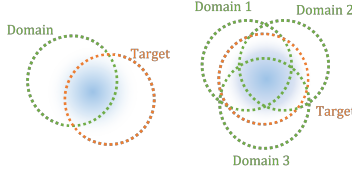


Figure 1: A multi-source domain has the potential to provide more adequate generic features than a single source domain.

such as contours, textures, and shadows. Some combination of multiple source domains with different similarities to the target domain has the potential to provide sufficient knowledge [43, 44], Multi-source transfer learning integrates the rich knowledge of multiple source domains, which can avoid the problem of insufficient features provided by a single source domain, and reduce the impact of negative transfer[45] as shown in Figure 1. One idea is to perform multi-source transfer learning [46] at the data level, and some work [47, 48, 49] assigns different weights from different source domains according to the overall similarity between the source domain and the target domain. There is also work [45] to select the most appropriate sample reweighting in multiple source domains. Another idea is to perform multi-source transfer learning at the model level. For example, multiple models are independently trained using different source domains, and the optimal model[50, 51, 52] is selected for the task through the similarity measurement between each source domain and the target domain or according to the performance of the task. Or when facing a classification problem, vote [53] for all model outputs to determine the final output. Some jobs [54, 55] also design different weights for different models. Some recent works use pseudo-labels to induce domain adaptation in multiple source domains. This self-training strategy with pseudo-target labels can enhance the cross-domain capabilities of source classifiers. Methods have been developed for the data [56] and the model [57]. The literature [58] has applied multi-source transfer learning to liver cancer ultrasound images. To sum up, if natural images are used as the source domain, it is possible to extract features that are not related to the target

domain, and other tissues/organs can be used for cross-modal migration. However, the ultrasound image itself has less information, and the transferable information that can be extracted is limited. Multiple source domains of ultrasound images with similar local features can be used for multi-source transfer learning to complement the lack of key features. Although ultrasound image datasets generally have the characteristics of small labeled samples, there are a large number of unlabeled ultrasound images available, so adversarial transfer learning can be used to utilize these large batches of unlabeled data. Multi-source adversarial transfer learning combines the advantages of adversarial transfer learning and multi-source transfer learning. Compared with other multi-source transfer learning, it adaptively extracts common features in multiple source domains through adversarial thinking, while providing the possibility to utilize unlabeled target domain data. Compared with adversarial transfer learning, multiple source domains avoid the problem of insufficient general features provided by a single source domain. At present, multi-source adversarial transfer learning has relatively mature solutions in classification problems, time series prediction, etc., and some people have used it in building energy prediction[55], and blood glucose prediction[42]. There are relatively few applications in the field of medical image segmentation.

To this end, a multi-source adversarial transfer learning image segmentation network for ultrasound image segmentation is proposed. Common features are extracted between multiple source domains and target domains through adversarial transfer learning to solve the insufficient target domain data labeling. Through the multi-source fusion strategy, the problem of insufficient key features provided by a single source domain is solved. Specifically, four components are included: feature extractor, domain classifier, feature fuser, and segmentation predictor (including source and target domains). The feature extractor is composed of a downsampling layer, which can extract deep transferable features between domains, and provide the learned transferable features to the domain classifier and feature fusion. The domain classifier works by distinguishing the features input by the feature extractor from the source domain or the target

domain, and encourages the feature extractor to learn cross-domain representations through a gradient inversion layer. The feature fuser fuses the information from each feature extractor and provides it to the segmentation predictor. The segmentation predictor takes common features from the feature extractor and learns meaningful representations from the transferable features present in the source and target domains, respectively, to perform the segmentation task. The main contributions of this paper can be summarized as follows:

1. To the best of our knowledge, this work is the first attempt to apply multiple source-domain guidance across tissues/organs to help solve the problem of target domain ultrasound image segmentation with insufficient label data.
2. We propose a multi-source adversarial transfer learning image segmentation framework and its training method, which integrates multiple adversarial transfer learning sub-networks to solve the problem that a single source domain with limited similarities cannot provide sufficient knowledge.
3. We design a multi-source domain-independent strategy to further enhance the network's transfer learning ability by improving the distribution estimation of the target domain and maintaining data balance while maximizing the use of source domain data.

The rest of this article is organized as follows. Section II details the proposed method and its background. The experimental results can be found in Section III. The conclusions are contained in Section IV.

2. METHODS

2.1. Problem formulation

Given a target domain dataset $\mathcal{D}_t = \mathcal{D}_{t_l} \cup \mathcal{D}_{t_u} = \{x_j, y_j\}_{j=1}^{n_{t_l}} \cup \{x_j\}_{j=n_{t_l}+1}^{n_{t_l}+n_{t_u}}$, where, x_j is the target domain image, y_j is the target domain mask, n_{t_l} images in \mathcal{D}_{t_l} have masks, n_{t_u} images in \mathcal{D}_{t_u} have no masks, the dataset \mathcal{D}_t has a total of $n_t = n_{t_l} + n_{t_u}$ samples. Also given a set of source domains with N source domains $\mathcal{D}_s = \{\mathcal{D}_{s_i}\}_{i=1}^N$, each source domain has n_{s_i} images with all pixel-level image labels, denoted as $\mathcal{D}_{s_i} = \{x_j^i, y_j^i\}_{j=1}^{n_{s_i}}$, where x_j^i is the

source domain image, y_j^i is the image mask at the pixel level of the source domain. The source domain and target domain come from different but related domains, such as ultrasound images of different organs, or images acquired by different models of ultrasound instruments. The task considered is to transfer knowledge from N ultrasound image source domains with sufficient data $\mathcal{D}_{s_i} = \{x_j^i, y_j^i\}_{j=1}^{n_{s_i}}$ fusion to the target domain of ultrasound images with insufficient annotation data $\mathcal{D}_t = \{x_j, y_j\}_{j=1}^{n_{t_l}} \cup \{x_j\}_{j=n_{t_l}+1}^{n_{t_l}+n_{t_u}}$ to improve segmentation prediction results. Since the ultrasound images of each source domain and target domain are affected by different acquisition equipment and different source organs, their marginal probabilities present different distributions: $P(\mathcal{D}_t) \neq P(\mathcal{D}_{s_1}) \neq \dots \neq P(\mathcal{D}_{s_i}) \neq \dots \neq P(\mathcal{D}_{s_n})$. Therefore, the goal of multi-source adversarial transfer learning is to learn the transformation function F_T^i by adversarial, let $P(F_T^i(\mathcal{D}_t)) = P(F_T^i(\mathcal{D}_{s_i}))$, this function will be used to the segmentation predict function $\mathcal{F}_P(\cdot)$, in this form $\mathcal{F}_P(\cdot) = \mathcal{F}_P(F_T^i(\cdot))$ complete the unsupervised domain of each source domain and target domain adapt to work.

2.2. The architecture

As shown in the figure2, unlike most current transfer learning methods where the source domain and the target domain share the entire model parameters, our method designs a separate sub-network for each source domain. The purpose of this is to keep the source domains independent of each other. Since the semantic information of the domains is not exactly the same, such as different types of diseases, it means that there is only partial similarity between them, and only some local features can be transferred. We hope to fuse these local features through multiple source domains to complete all the required features as much as possible. If all the parameters of the network are shared, the source domains will affect each other, so it is necessary to keep the source domains independent of each other. The feature extractor is considered by us to be the most critical part of deep learning, because accurate extraction of available features is the basis for the task of the later task layer. Our idea is to extract the parts

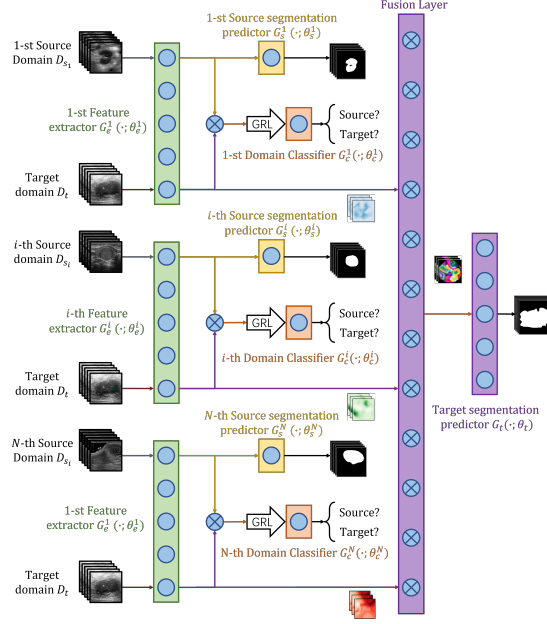


Figure 2: Multiple Sub-networks use the feature fusion layer to form the Structure multi-source adversarial transfer learning network.

that are common to each source and target domain as much as possible, while keeping them as individual as possible to guarantee complementary effectiveness. Therefore, as shown in Figure 4, in addition to a separate feature extractor, the sub-network also designs a separate source domain segmentation predictor. The parameters of each source domain and target domain are shared pairwise, and no parameters are shared between source domains at the feature extractor and source domain segmentation predictor levels. Therefore, we think that what the sub-network adaptively extracts is the local features that are common between the source domain and the target domain, rather than the features that are common between all domains.

First, the sub-network of adversarial transfer learning is introduced. The main parts of the sub-network for image segmentation are the feature extractor and the segmentation predictor, which are mainly inspired by U-net, as shown in Figure 3, in which the encoding part performs the feature map. Down-sampling

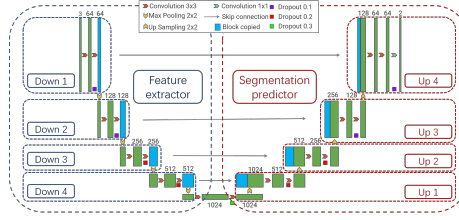


Figure 3: U-Net has the structure of the Down-sampling Encoding, Up-sampling Decoding and Jumping Connection, which combines a more detailed graphic and deep features that help target classification.

to obtain more abstract semantic features and then to judge the category of objects; The decoding part performs Up-sampling step by step, and at the same time receives the information copied from the encoding part, and finally restores the image gradually.

The adversarial transfer learning network is inspired by the generative adversarial network [59], and the structure is generally composed of a feature extractor, an output predictor, and a domain classifier. The common features of the source and target domains are adaptively extracted, and the common features are used as the input of the target predictor to achieve the purpose of task performance optimization in the target domain, and also provide the possibility to maximize the use of unlabeled target domain data. As shown in Figure 4, the proposed multi-source adversarial transfer learning sub-network is divided into four parts: Feature extractor $G_e^i(\cdot; \theta_e^i)$, Domain classifier $G_c^i(\cdot; \theta_c^i)$, Target segmentation predictor $G_t(\cdot; \theta_t)$ and Source segmentation predictor $G_s^i(\cdot; \theta_s^i)$ where θ_e^i , θ_c^i , θ_t and θ_s^i are parameters. In the vertical direction, the upper and lower parts of the Feature extractor $G_e^i(\cdot; \theta_e^i)$ correspond to the source and target domains, respectively, and share all parameters, this part is equivalent to the same network, the image can obtain deep features after passing through the feature extractor; The Domain classifier $G_c^i(\cdot; \theta_c^i)$ judges whether the input comes from the source domain or the target domain according to the deep features of the input; The Source segmentation predictor $G_t(\cdot; \theta_t)$ and the Target segmentation predictor $G_s^i(\cdot; \theta_s^i)$ have the same structure, also accept the deep

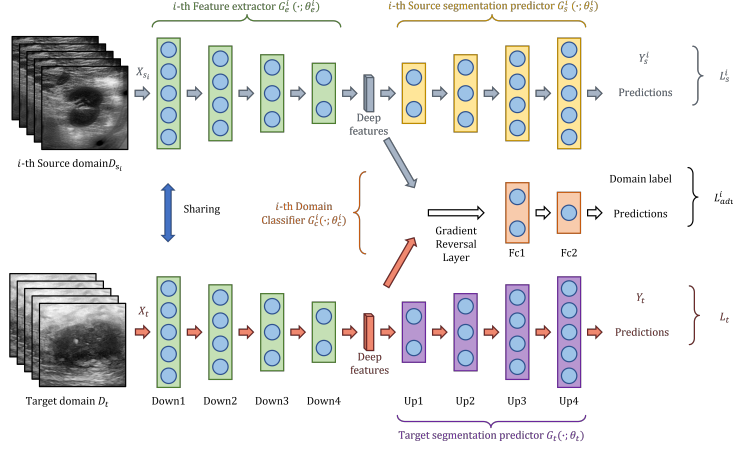


Figure 4: The i -th Sub-network consists of the i -th Feature extractor $G_e^i(\cdot; \theta_e^i)$, the i -th Domain Classifier $G_c^i(\cdot; \theta_c^i)$, the i -th Source segmentation predictor $G_s^i(\cdot; \theta_s^i)$, and the Target segmentation predictor $G_t(\cdot; \theta_t)$

features from the feature extractor and output the predicted segmentation, but their training is done separately, as it is ensured that the tasks of the source and target domains cannot influence each other at the level of the segmentation predictor. Specifically, the source segmentation predictor $G_s^i(\cdot; \theta_s^i)$ accepts the corresponding source domain data from this subnetwork. The target segmentation predictor $G_t(\cdot; \theta_t)$ accepts data from the target domain. Table 1 describes each predefined layer.

As shown in Figure 2, the overall network includes N sub-networks, and it is necessary to comprehensively utilize the deep features of each network using the fusion feature [60]. The purpose of this is to independently learn complementary information from different domains. The depth features output by multiple feature extractors have chosen a fusion method similar to the add in the literature [61], sums abstract features from different sub-networks to make the model easier to train with less data in the target domain. The abstract features extracted by the feature extractors of multiple sub-networks will be fused in the segmentation predictor fusion layer in the target domain. Specifically, we separate out the first upsampling layer of the target domain segmentation

Table 1: The structure definition of each layer in the network structure

Structure	Layer type	F/S ^a	P/S ^b	A/U ^c
	MaxPool2d	2×2	-	-
Down	Conv2d	3×3	1	ReLU
	Conv2d	3×3	1	ReLU
	Upsample	-	2	Bilinear
Up	Conv2d	3×3	1	ReLU
	Conv2d	3×3	1	ReLU
	Linear	-	-	ReLU
Fc	Linear	-	-	ReLU

^a F/S = Filter/Stride size^b P/S = Padding / Scale factor^c A/U = Activation function / Upsampling algorithm

predictor in Figure 5 to form a feature fusion layer. The fusion layer can be regarded as the transformation $g_1(\cdot) = W_1(\cdot)$, where W_1 is the parameter that needs to be learned. We let the abstract features $\mathcal{X}_i \big|_{i=1}^N$ from all sub-networks be summed in front of it. Then a new feature map \mathcal{X}^1 is obtained through the fusion layer.

$$\mathcal{X}^1 = g_1 \left(\sum_{i=1}^N \mathcal{X}_i \right) = W_1 \left(\sum_{i=1}^N \mathcal{X}_i \right) \quad (1)$$

The premise of being able to use this summation method is that the input data of each sub-network is exactly the same. Through the multi-source domain independent strategy designed later, we ensure that each batch of target domain data passing through each feature extractor is exactly the same. Then, after the same batch of data from the target domain passes through all sub-networks, the abstract features extracted from the same batch of data are fused in the form of summation. Then enter the second upsampling layer $g_2(\cdot)$, The third upsampling layer $g_3(\cdot)$, the fourth upsampling layer $g_4(\cdot)$, output the predicted segmentation results. The parameters of each layer of the prediction segment $W_k \big|_{k=1}^4$ will be updated by the marked target domain data, and all parameters will be recorded as θ_t :

$$\theta_t = \{W_1; W_2; W_3; W_4\} \quad (2)$$

The contribution of each source domain is implicit, because each sub-network extracts the transferable features between the corresponding source domain and the target domain during the training process through the method of adversarial transfer learning. We consider the contribution of each source domain to be determined by their similar characteristics to the target domain.

2.3. Multi-domain independence strategy

Since the multi-source adversarial transfer learning includes the adversarial Domain classifier $G_c^i(\cdot; \theta_c^i)$, it inputs the deep features extracted by the Feature extractor $G_e^i(\cdot; \theta_e^i)$ from the source domain \mathcal{D}_{s_i} and the target domain \mathcal{D}_t . To ensure the adversarial effect, data balance is also very important. Because in some cases the target domain data sample size $n_t = n_{t_l} + n_{t_u}$ is usually much smaller than the source domain data sample size n_{s_i} , if we directly mix the data of the two domains and generate batches of size n^b , then the expected number of source domain images $E(n_{s_i}^b)$ is Eq.(3), the expected number of target domain images $E(n_t^b)$ is Eq.(4).

$$E(n_{s_i}^b) = n^b \times \frac{n_{s_i}}{n_t + n_{s_i}} \quad (3)$$

$$E(n_t^b) = n^b \times \frac{n_t}{n_t + n_{s_i}} \quad (4)$$

Since $n_{s_i} \gg n_t$, so $E(n_{s_i}^b) \gg E(n_t^b)$. This data imbalance not only affects the learning efficiency of the target domain network, but also causes the performance of the domain classifier to degrade, which in turn affects the feature extractor's ability to extract general-purpose deep features.

In addition, since all sub-networks in multi-source adversarial transfer learning are trained at the same time, it is necessary to ensure that the data from the target domain that each batch passes through each sub-network is the same, because they share the same target segmentation predictor after passing through the feature fusion layer. In most cases, the number of samples n_{s_i} is different for each dataset \mathcal{D}_{s_i} as the source domain. If the minimum number of source domain samples is used as the benchmark, this will lead to a large amount of valuable source domain data being wasted.

Domain-independent strategy [62] is a method we proposed in the past to solve the problem of data imbalance. In addition to ensuring data balance, this method can more reliably represent the overall distribution of target domain data. The idea of this method is to select the same number of samples in both domains to form batch data while keeping the source and target domains independent. In this case, not only the mathematical expectation of the number of samples in the source domain $E(n_{s_i}^b)$ and the mathematical expectation of the number of samples in the target domain $E(n_t^b)$ can be the same in the batch data, but also because of the increase in the target domain data, the target domain in the batch data is also increased. The sample distribution is also closer to the overall distribution:

$$E(n_{s_i}^b) = E(n_t^b) = \frac{n^b}{2} \quad (5)$$

In this paper, to further solve the problem of waste caused by the different amounts of data in each source domain, we regard the batch data generated by the previously proposed strategy as a sub-batch data, generate N sub-batches of data for N source and target domains, and then treat them as one batch. This generalizes this strategy from the previous single source domain to multiple source domains. At this time, the number of batch samples n^b in Eq.(5) should be rewritten as the number of sub-batch samples n^{sb} , and it should be guaranteed that:

$$E(n_{s_1}^{sb}) = \dots = E(n_{s_N}^{sb}) = E(n_t^{sb}) = \frac{n^{sb}}{2} \quad (6)$$

Since each source domain is combined with the target domain into a sub-batch, the real batch size should be:

$$n^b = N \times n^{sb} \quad (7)$$

Specifically, as shown in Figure 5, the same number of samples should be selected in each domain to form batch data while all source and target domains remain independent, and all data should be guaranteed to be used.

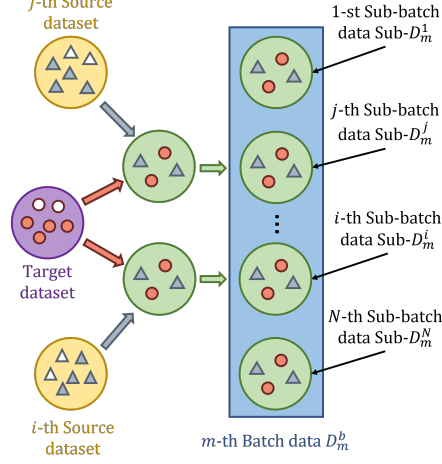


Figure 5: Generate multiple Sub-batch data with the Multi-domain independence strategy and then constitute the batch data.

2.4. Loss function

In terms of the loss function of adversarial transfer learning between the target domain and the i -th source domain s_i , The target domain task is to require the target image to perform as best as possible in segmentation, and the optimization goal should be:

$$\arg \min (L_t^i) = \arg \min (L_t^i (G_t^i (G_e^i (\cdot; \theta_e^i); \theta_t))) \quad (8)$$

Similarly, the optimization objective of the i -th source domain s_i should be:

$$\arg \min (L_s^i) = \arg \min (L_s^i (G_s^i (G_e^i (\cdot; \theta_e^i); \theta_s^i))) \quad (9)$$

The purpose of adversarial is to extract general features, and the domain classifier is required to be as indistinguishable as possible from the source of the extracted features. The optimization goal should be:

$$\arg \max (L_{adv}^i) = \arg \max L_{adv}^i (G_c^i (G_e^i (\cdot; \theta_e^i); \theta_c^i)) \quad (10)$$

To unify the form with the segmentation task to facilitate the solution, it should be written in the form of $\arg \min L_{adv}^i$. According to the literature [33], a Gradient

Reversal Layer (GRL) is introduced to multiply the gradient by some negative constant (such as a negative identity matrix $-I$) during backpropagation-based training. The form of adversarial transfer learning optimization objective for a single source domain versus the target domain is:

$$\arg \min (\mathcal{L}_i) = \arg \min (L_s^i + \alpha L_t^i - \lambda L_{adv}^i) \quad (11)$$

Since the target domains in the same batch may not all have labels, the above formula needs to be refined for the batch, and then the overall loss function can be obtained. First, starting from the sample level, let the sample X_j come from the source domain D_{s_i} , that is, $X_j \in \mathcal{D}_{s_i}$, then the loss function for this sample is:

$$\begin{aligned} \mathcal{L}_i(X_j) &= L_s^i - \lambda L_{adv}^i \\ &= L_s^i (G_s^i (G_e^i (X_j; \theta_e^i); \theta_s^i)) \\ &\quad - \lambda L_{adv}^i (G_c^i (G_e^i (X_j; \theta_e^i); \theta_c^i)) \end{aligned} \quad (12)$$

Similarly, if the sample comes from the labeled target domain, that is, $X_j \in \mathcal{D}_{t_l}$, the loss function for this sample is:

$$\begin{aligned} \mathcal{L}_i(X_j) &= L_s^i - \lambda L_{adv}^i \\ &= L_s^i (G_t (G_e^i (X_j; \theta_e^i); \theta_t)) \\ &\quad - \lambda L_{adv}^i (G_c^i (G_e^i (X_j; \theta_e^i); \theta_c^i)) \end{aligned} \quad (13)$$

Assuming that the sample comes from the marked target domain $X_j \in \mathcal{D}_{t_u}$, the loss function for this sample is:

$$\begin{aligned} \mathcal{L}_i(X_j) &= -\lambda L_{adv}^i \\ &= -\lambda L_{adv}^i (G_c^i (G_e^i (X_j; \theta_e^i); \theta_c^i)) \end{aligned} \quad (14)$$

Integrate Eq.(12), Eq.(13), and Eq.(14), the loss function for a single sub-batch $Sub-D_m^i$ containing the i -th source domain, the labeled target domain, and the unlabeled target domain is:

$$\begin{aligned} \mathcal{L}_b^i &= \sum_{X_j \in (Sub-D_m^i \cap \mathcal{D}_{s_i})} L_s^i (G_s^i (G_e^i (X_j; \theta_e^i); \theta_s^i)) \\ &\quad + \alpha \sum_{X_j \in (Sub-D_m^i \cap \mathcal{D}_{t_l})} L_t (G_t (G_e^i (X_j; \theta_e^i); \theta_t)) \\ &\quad - \lambda \sum_{X_j \in Sub-D_m^i} L_{adv}^i (G_c^i (G_e^i (X_j; \theta_e^i); \theta_c^i)) \end{aligned} \quad (15)$$

Combined with (15) generalizing the number of source domains from 1 to N , the loss function for all source domains is:

$$\begin{aligned}
\mathcal{L} &= \sum_{i=1}^N \mathcal{L}_b^i \\
&= \sum_{i=1}^N \sum_{X_j \in (Sub-D_m^i \cap \mathcal{D}_{s_i})} L_s^i(G_s^i(G_e^i(X_j; \theta_e^i); \theta_s^i)) \\
&\quad + \alpha \sum_{X_j \in (Sub-D_m^i \cap \mathcal{D}_{t_i})} L_t \left(G_t \left(\sum_{i=1}^N G_e^i(X_j; \theta_e^i); \theta_t \right) \right) \\
&\quad - \lambda \sum_{i=1}^N \sum_{X_j \in Sub-D_m^i} L_{adv}^i(G_c^i(G_e^i(X_j; \theta_e^i); \theta_c^i))
\end{aligned} \tag{16}$$

2.5. The learning process

The purpose of the proposed multi-source adversarial transfer learning is to extract the common underlying features of each source domain D_{s_i} and target domain D_t in the source domain set $D_s = \{D_{s_i}\}_{i=1}^N$ in an adversarial manner. The domain-independent strategy is extended to multiple source domains to ensure that each valuable source domain data is not wasted while ensuring balanced learning of each sample in each source domain and target domain. For training this network, the idea is to train multiple Feature extractors $G_e^i(X_j; \theta_e^i)$ to extract deep features. For general feature extraction, data from the source domain and the target domain will be given Domain Labels, and then enter the Domain classifier $G_c^i(G_e^i(X_j; \theta_e^i); \theta_c^i)$ to complete the domain adaptation. The sub-batch data from the source domain trains the Source segmentation predictor $G_s^i(G_e^i(X_j; \theta_e^i); \theta_t)$ of the sub-network after the feature extractor and obtains the result of the source domain image segmentation. The sub-batch data from the target domain is extracted and the Target segmentation predictor $G_t \left(\sum_{i=1}^N G_e^i(X_j; \theta_e^i); \theta_t \right)$ of the sub-network is trained, and the result of the target domain image segmentation is obtained. Therefore, the optimization objective is:

$$\left\{ \hat{\theta}_e^i; \hat{\theta}_t; \hat{\theta}_s^i; \hat{\theta}_c^i \right\}_{i=1}^N = \min_{\Theta} (\mathcal{L}(\Theta)) \tag{17}$$

Where, $\Theta = \{\theta_e^i; \theta_t; \theta_s^i; \theta_c^i\}_{i=1}^N$ is the network parameter, $\hat{\Theta} = \{\hat{\theta}_e^i; \hat{\theta}_t; \hat{\theta}_s^i; \hat{\theta}_c^i\}_{i=1}^N$ is the estimated parameter of the network. After the network is trained, the learned transformation function is $F_T^i = G_e^i(\cdot; \theta_e^i)$, which can extract common

features between the source and target domains. Segmentation predict function $F_P = G_t(\cdot; \theta_t)$ utilizes the learned general features and has good generalization ability. Finally, the prediction function can be directly applied to the segmentation prediction task of the target ultrasound image.

$$\widehat{\mathcal{F}}_P(\cdot) = G_t \left(\sum_{i=1}^N G_e^i(\cdot; \theta_e^i); \theta_t \right) \quad (18)$$

The specific implementation steps are shown in the algorithm 1

Algorithm 1 Multi-source Adversarial Transfer Learning Algorithm

Input:

The source datasets, $D_s = \{D_{s_i}\}_{i=1}^N$, Where, $D_{s_i} = \{x_j^i, y_j^i\}_{j=1}^{n_{s_i}}$;

The target dataset, D_t , Where, $D_t = \{x_j, y_j\}_{j=1}^{n_{t_l}} \cup \{x_j\}_{j=n_{t_l}+1}^{n_{t_l}+n_{t_u}}$;

Total epoch, e_{total} ;

Sub-batch size, n^{sb} ;

1: Multi-domain independence strategy

2: **for** $e = 1; e \leq e_{total}; e++$ **do**

3: **for** $m = 1; m \leq \max(n_{s_i}|_{i=1}^N)/n^{sb}; m++$ **do**

4: **for** $i = 1; i \leq N; i++$ **do**

5: Extract deep features $G_e^i(X_m^i; \theta_e^i)$ from the batch dataset D_m^i

6: Get predictions $G_s^i(G_e^i(X_m^i; \theta_s^i); \theta_d^i)$, $G_t(G_e^i(X_m^i; \theta_e^i); \theta_t)$ and $G_c^i(G_e^i(X_m^i; \theta_e^i); \theta_c^i)$;

7: **end for**

8: Calculate the loss function as Eq.(16);

9: Backpropagation to update the network parameters $\Theta = \{\theta_e^i; \theta_t; \theta_s^i; \theta_c^i\}_{i=1}^N$ from \mathcal{L}_b ;

10: **end for**

11: **end for**

Output:

Deep prediction model, $\widehat{\mathcal{F}}_P(\cdot) = G_t \left(\sum_{i=1}^N G_e^i(\cdot; \theta_e^i); \theta_t \right)$;

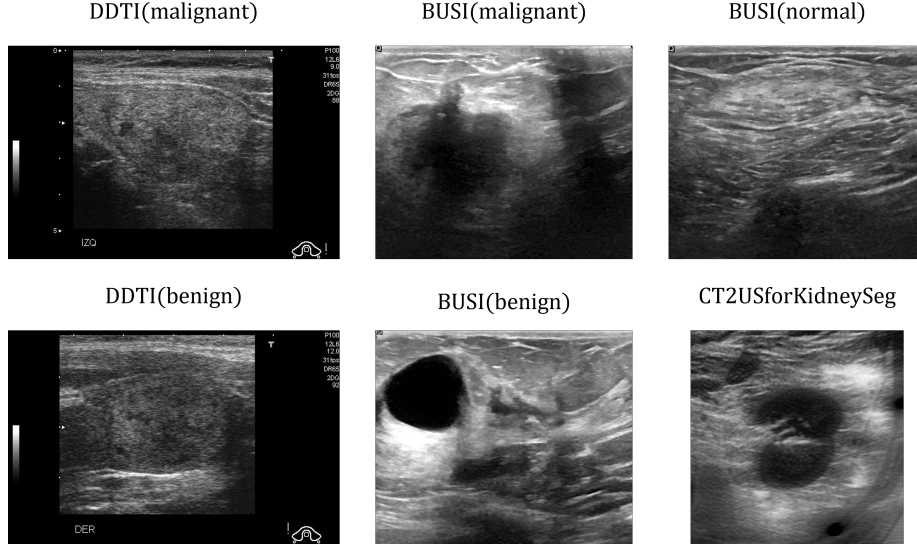


Figure 6: Examples of 6 types of raw data in the Breast Ultrasound Images Dataset, DDTI Dataset and CT2USforKidneySeg Dataset.

3. EXPERIMENTAL RESULTS AND ANALYSIS

3.1. Dataset description

In this paper, ultrasound images from three datasets are used to test the performance of multi-source adversarial transfer learning in ultrasound image segmentation, involving organs including the breast[63](Breast Ultrasound Images Dataset, Dataset BUSI), Thyroid (DDTI) [64] and kidney (CT2USforKidneySeg) [25], their unprocessed raw examples are shown in Figure 6, and these datasets are described below.

3.1.1. Breast Ultrasound Images Dataset

The BUSI dataset [63] was collected in 2018 and includes breast ultrasound images of 600 women between the ages of 25 and 75. The dataset consists of 780 images in PNG format with an average image size of 500×500 pixels. The images are divided into three categories: normal, benign and malignant, with 133, 437 and 210 images, respectively. In this paper, the main work is

ultrasound image segmentation, so the normal image should be removed. Due to the large gap between benign and malignant in terms of boundary and texture in appearance, combined with the previous work, this dataset was disassembled for segmentation work[65],[66], this work regards benign and malignant as two fields: BUSI(Benign) and BUSI(Malignant), respectively.

3.1.2. *Digital Database of Thyroid Ultrasound Images*

The DDTI dataset[64] is an open-access resource for the scientific community. Support for this project was provided by the National University of Colombia, CIM@LAB and IDIME (Instituto de Diagnostico Medico). The main purpose of the dataset DDTI is to develop algorithms for applying CAD systems to the analysis of thyroid nodules, containing annotations and patient diagnostic information for manually labeled suspicious lesions using the TI-RADS classification by experienced radiologists. The dataset consists of raw thyroid images of size 560×360 pixels, and the pixel labels of the tumor contour regions are given in the corresponding XML files. When performing the segmentation task, the XML tag should be converted into a mask before it can be used. The DDTI dataset contains 390 cases with 91 normal, 52 benign, and 247 malignant categories, and some single cases have multiple view images. It can be seen from the image examples that benign and malignant images are very close in appearance, and in the previous work [67], [68], for the segmentation task, the benign and malignant images in the dataset are mixed. Therefore, in the following text, the two sub-datasets in this dataset will be regarded as the same source domain, abbreviated as DDTI.

3.1.3. *CT2USforKidneySeg*

The CT2USforKidneySeg dataset is a dataset provided by the literature [25], which uses labeled real CT data and some ultrasound data to synthesize more ultrasound images to construct a transition dataset, and then migrate to real ultrasound images for segmentation. The dataset has a total of 4,586 samples and is simply called Kidney.

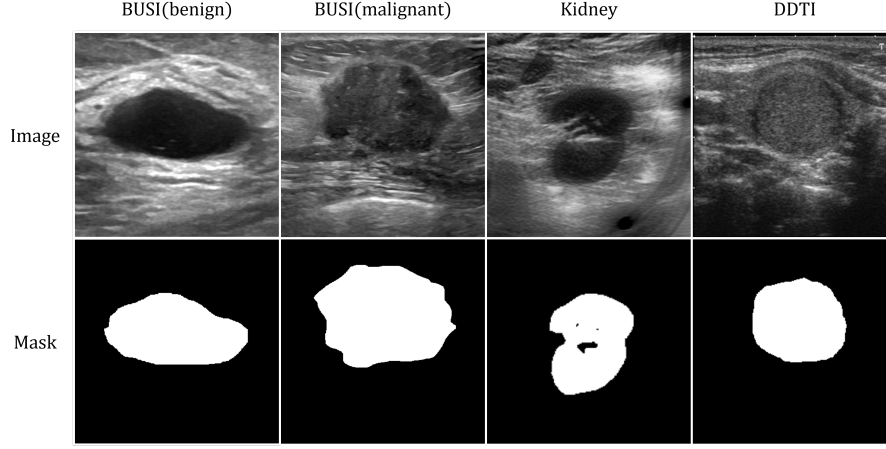


Figure 7: An example of the processed data image of the four domains, including scaling to the same size, removing black borders, removing text, and generating a mask from an XML file.

3.2. Data preprocessing

In terms of data preprocessing, due to the presence of black borders and text in some data, the performance of the algorithm will be degraded if used directly, so the black borders and text should be deleted during processing; For the dataset, firstly, the target domain dataset is divided into training set, validation set and test set according to the ratio of 0.8 : 0.1 : 0.1. Since transfer learning focuses on tasks in the target domain, there is no need to divide the source domain dataset into a test set. Due to the limitation of computing resources, the amount of data in each batch in the image segmentation task is small, so the method of group normalization [69] is adopted to normalize the data to achieve a better segmentation effect. Examples of images in the processed dataset are shown in Figure 7.

3.3. Experimental indicators

After each pixel passes through the network, it will output the predicted classification label, TP , FP , TN , FN which are four kinds of results, indicate true positive, false positive, true negative, and false negative, respectively. In

general, for the segmentation problem of each image, different test indicators can be selected according to different focuses. The most common indicator is the *IOU* score (Intersection over Union), which can be understood as the real correct area and the prediction as correct. The *IOU* is calculated as follows:

$$IOU = \frac{TP}{FP + FN} \quad (19)$$

In addition to the *IOU* score indicator, *Precision* and *Recall* are two commonly used basic indicators. Among them, the *Precision* score is the ratio of the number of correctly predicted true positive pixels to the total number of predicted positive pixels (from the perspective of the prediction result, how many predictions are accurate), focusing on finding the right ones; The *Recall* score is the ratio of the correctly predicted true positive pixels to the total number of true positive pixels (from the perspective of true annotation, how many are recalled), focusing on finding all. They are defined as follows:

$$Precision = \frac{TP}{TP + FP} \quad (20)$$

$$Recall = \frac{TP}{TP + FN} \quad (21)$$

However, sometimes the target task needs to comprehensively consider the *Precision* score and the *Recall* score, and the F_β score comes into being. Its calculation method is as follows:

$$\begin{aligned} F_\beta &= (1 + \beta^2) \times \frac{Precision \times Recall}{(\beta^2 \times Precision) + Recall} \\ &= \frac{(1 + \beta^2) \times TP}{(1 + \beta^2) \times TP + \beta^2 \times FN + FP} \end{aligned} \quad (22)$$

Among them, β can take different values according to the focus of the task indicator. When β taken 1, it is the F_1 score, which is the famous *Dice* score; other values can also be taken, such as the F_2 score and the $F_{0.5}$ score, where F_2 The score indicates that recall is weighted more than precision and the $F_{0.5}$ score indicates that precision is weighted more than recall.

At the pixel level of each sample, the test indicators selected in this paper are as follows, namely *IOU*, *Dice*, F_2 and $F_{0.5}$. The above test indicators are

Table 2: Parameters setting

Items	Parameters setting
Prediction loss	Cross-Entropy
Total epochs	100
Batch size	16
Optimizer	Root Mean Square Prop(RMSprop)
Learning rate	[0.001,0.0001]

only for specific images in the data set. To reflect the situation of the entire data set, it is necessary to test all the images, and then take the mean and standard deviation as the data to prove the experiment.

3.4. Experimental parameter settings

By observing each data set, it can be seen that the background texture of BUSI(Benign) and BUSI(Malignant) is similar to that of the target Kidney’s boundary and texture, so BUSI(Benign) can be selected as the target domain, BUSI(Malignant) as the source domain 1 and Kidney as the source domain 2; In addition, the background textures of BUSI(Malignant) and BUSI(Benign) are similar, as well as the target demarcation lines and textures of DDTI, so BUSI(Malignant) as the target domain, BUSI(Benign) as the source domain 1 and DDTI as the source domain 2. In terms of experimental parameter setting, Pytorch is selected as the deep learning framework, and the random seed is set to 0 to avoid accidentality during model training, as shown in table 2, experiment with them separately. In order to intuitively reflect the performance change when the proportion of unlabeled data rises from 0% to 90% in the later experiments, we plot the trend of IOU , $Dice\ score$, F_2 and $F_{0.5}$ results for all experiments.

3.5. Compare experimental results and analysis

In terms of comparative experiments, this work selected some common multi-source transfer learning methods described above and compared them with the

proposed method. At the data level, [47] is selected to assign different weights to different source domain data as *Comparison₁*. At the model level, we chose [50] for multi-model domain adaptation as *Comparison₂*. In addition, we tested also assigning different weights to different source domain models according to the similarity of the dataset. Simultaneously all model outputs are tested by voting method [53] as *Comparison₃*. We assign pixel-level pseudo-labels [56] to some data, and then try to do domain adaptation as *Comparison₄*.

3.5.1. BUSI(Benign) Comparative Experiment Results and Analysis

We tested the performance metrics *IOU*, *Dice score*, F_2 and $F_{0.5}$ on the BUSI(Benign) dataset with different proportions of unlabeled data. The results are shown in the table 3. Figure 8 plots the trend of all experiments in the table 3 as the proportion of unlabeled data increases from 0% to 90%. It can be seen that among the four indicators, *Proposed Method* has the best performance. The method *Comparison₁* of assigning different weights to the data has the worst effect. We believe that this is because the overall similarity is insufficient, and simply weighting the data cannot filter out the desired features at the local feature level. The performance of *Comparison₂* and *Comparison₃* at the model level is close to that of the pseudo-label-based method *Comparison₄*. We believe that the multi-source transfer learning and pseudo-label methods at the model level are feasible. However, the overall similarity between domains in this work is limited, and we believe that these methods may not be well suited to handle such scenarios where there are only partial similarities between the source domain and each target domain.

3.5.2. BUSI(Malignant) comparative experiment results and analysis

Similar to the comparison experiment of BUSI (Benign), the figure 9 draws the trend of the table 9. Also similar to the comparison experiment of BUSI (Benign), *Proposed Method* has the best performance. The method *Comparison₁* that assigns different weights to the data is the worst. It is worth noting that for this data set, *Comparison₁*, *Comparison₂* and *Comparison₃* have a signif-

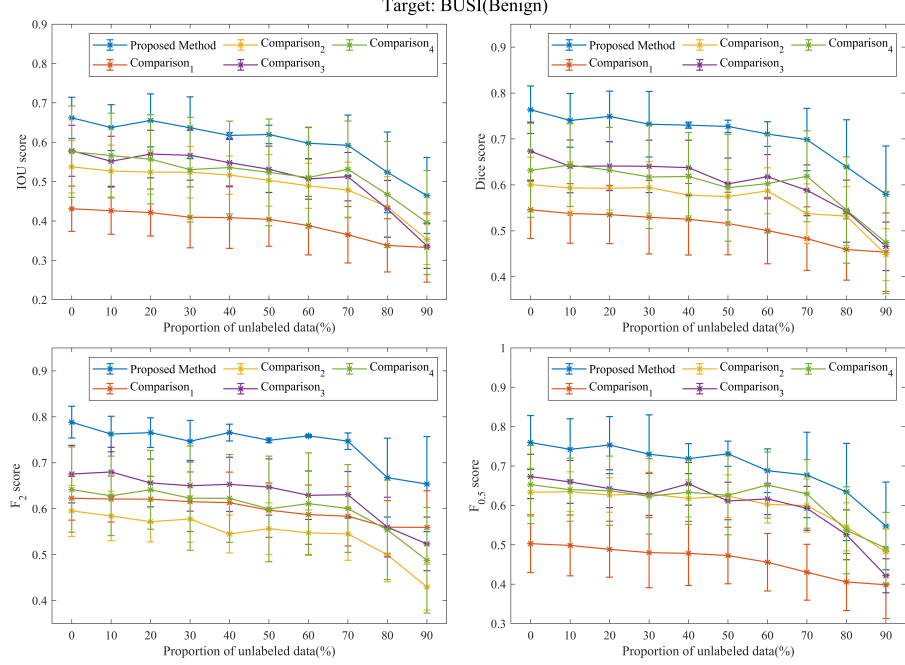


Figure 8: The method comparison experiment using BUSI (Benign) as the target domain, and BUSI (Malignant) and CT2US as the two source domains. The curves of the four indicators of IOU , $Dice$ score, F_2 and $F_{0.5}$ as a function of the proportion of unlabeled data are plotted.

icant performance drop when the unlabeled data reaches about 70%. And the performance drop of *Comparison₄* and *Proposed Method* has little change. We believe this is because these methods are better able to extract the key features needed to cover the target domain from the selected source domain than the experiments on the target domain BUSI (Malignant) compared to the experiments on the target domain BUSI (Benign).

3.6. Ablation experiment Results and Analysis

Since this paper uses adversarial transfer learning to solve the ultrasound image segmentation problem in the absence of labeled data, the core idea is to use adversarial transfer learning to extract common features between the source and target domains; However, considering that the common features provided

Target: BUSI(Benign)			Proportion of unlabeled data								
Score(%)	Experiment	0%	10%	20%	30%	40%	50%	60%	70%	80%	90%
I_{dU}	Proposed Method	66.197±5.239	63.725±5.832	65.545±6.714	63.68±7.845	61.718±0.76	61.986±2.343	59.749±3.998	59.216±7.682	52.359±10.259	46.45±19.653
	Comparison ₁	43.108±5.751	42.594±5.963	42.142±5.964	40.926±7.735	40.847±7.82	40.807±6.848	38.813±7.424	36.495±7.179	33.79±6.755	33.274±8.798
	Comparison ₂	53.76±6.657	52.681±6.578	52.399±5.602	52.357±6.544	51.653±4.88	50.31±5.554	48.923±5.728	47.848±7.089	43.595±7.655	35.288±6.335
	Comparison ₃	57.832±6.481	55.157±6.365	57.904±6.029	56.695±6.325	54.792±5.92	53.124±5.889	50.681±5.154	51.239±6.15	43.072±7.224	33.659±5.692
$Dice$	Proposed Method	57.592±11.596	56.617±10.761	55.683±11.305	53.04±13.31	53.573±11.801	52.338±13.562	51.016±12.834	53.166±12.22	46.728±13.477	39.598±13.215
	Comparison ₁	76.361±5.16	74.044±5.86	74.893±5.53	73.212±7.127	72.99±0.663	72.743±1.347	71.055±2.694	69.868±6.797	63.931±16.241	57.94±10.355
	Comparison ₂	54.372±6.252	53.769±6.487	53.533±6.345	52.964±7.988	52.522±7.791	51.586±6.817	50.039±7.225	48.293±6.94	45.936±6.687	45.332±8.546
	Comparison ₃	60.049±5.985	59.345±5.701	59.284±4.754	59.429±5.627	57.76±4.517	57.449±5.906	58.704±5.002	53.722±6.496	53.177±6.426	44.602±5.671
F_2	Proposed Method	67.35±6.322	64.013±5.745	64.095±5.341	64.036±5.703	63.743±5.988	60.194±5.632	61.783±4.817	58.828±5.535	54.268±6.757	46.602±5.274
	Comparison ₁	63.163±10.244	64.317±9.007	63.191±9.33	61.722±11.222	61.831±9.557	59.379±11.64	60.266±10.72	61.873±9.888	54.532±11.58	47.44±11.125
	Comparison ₂	78.823±3.467	76.246±3.881	76.548±5.234	74.679±4.515	76.567±1.82	74.973±3.907	73.847±2.254	74.091±1.802	66.746±8.591	63.353±10.359
	Comparison ₃	62.266±4.771	62.113±4.99	62.075±4.981	61.512±6.489	61.317±6.465	59.674±5.919	58.698±6.455	58.354±6.475	55.974±5.803	55.927±7.985
$F_{0.5}$	Proposed Method	59.518±5.538	58.408±5.371	57.181±4.404	57.742±5.04	54.477±4.108	55.669±5.623	54.765±4.937	54.513±5.743	49.973±5.879	42.95±5.026
	Comparison ₁	67.525±6.279	68.001±5.358	65.615±5.203	64.987±5.509	65.29±5.911	64.706±6.129	62.925±5.27	63.032±5.05	55.988±6.503	52.341±5.831
	Comparison ₂	64.16±9.281	62.787±8.651	64.11±8.563	62.289±11.36	62.238±9.364	59.958±11.491	61.095±11.077	60.038±9.562	55.394±10.824	48.769±11.485
	Comparison ₃	75.992±6.84	74.245±7.76	75.338±7.253	73.013±9.96	71.873±9.621	73.123±2.217	68.812±5.543	67.723±19.848	63.422±12.396	54.763±11.119

Target: BUSI(Malignant)			Proportion of unlabeled data								
Score(%)	Experiment	0%	10%	20%	30%	40%	50%	60%	70%	80%	90%
I_{dU}	Proposed Method	67.177±4.149	64.422±1.358	64.154±11.891	62.906±11.746	63.08±8.387	62.168±7.378	62.521±8.765	61.352±11.598	61.907±9.248	60.841±9.704
	Comparison ₁	37.593±5.256	36.842±9.021	36.31±8.438	35.619±8.623	35.351±11.015	35.907±8.704	34.102±8.939	34.353±11.639	28.559±8.519	23.062±6.642
	Comparison ₂	43.432±4.141	42.044±7.176	39.392±6.903	39.625±6.796	40.075±5.594	39.537±7.833	40.326±5.92	38.531±5.861	34.549±5.982	28.392±8.439
	Comparison ₃	52.676±4.324	50.895±4.993	49.981±4.757	49.06±4.922	50.421±1.975	50.762±5.608	49.395±3.955	48.999±4.452	43.24±3.516	36.366±3.973
$Dice$	Proposed Method	53.573±11.761	52.992±11.317	51.696±9.811	51.625±11.798	51.391±12.25	51.383±13.144	51.352±14.601	50.975±14.081	49.537±12.015	46.731±11.539
	Comparison ₁	78.194±4.405	75.988±2.793	74.431±12.49	72.827±12.112	72.83±10.631	72.317±6.573	72.262±11.084	71.795±12.875	71.676±12.112	70.921±12.085
	Comparison ₂	46.818±6.131	45.726±12.52	47.218±10.543	44.39±11.417	45.505±14.991	44.893±11.496	44.177±12.207	40.72±16.461	35.712±12.937	28.759±11.397
	Comparison ₃	50.915±7.537	52.148±9.1	51.018±9.564	50.679±9.137	49.93±7.704	48.024±9.492	48.131±6.579	48.202±7.78	41.009±7.594	38.709±10.348
F_2	Proposed Method	66.127±4.124	64.121±4.575	62.568±4.679	63.095±4.666	61.318±2.136	64.137±5.519	62.755±4.574	62.458±3.45	55.474±4.553	50.701±4.439
	Comparison ₁	64.733±13.901	63.324±12.703	63.124±11.993	62.995±13.817	62.99±14.435	62.974±15.059	62.884±15.746	62.402±15.665	61.875±13.923	59.391±13.244
	Comparison ₂	81.505±5.605	80.462±2.965	75.952±8.46	73.144±9.648	70.675±9.604	73.262±4.19	71.033±9.51	68.938±12.816	71.17±10.811	69.753±9.883
	Comparison ₃	54.79±6.844	53.094±11.933	52.401±11.134	51.805±12.274	52.349±14.449	51.544±11.228	52.401±12.45	47.635±15.017	40.999±12.988	32.999±11.777
$F_{0.5}$	Proposed Method	54.246±9.955	53.143±10.782	53.282±11.48	52.714±11.683	48.947±10.289	49.714±12.451	49.091±10.066	50.503±11.732	46.165±9.914	38.435±13.155
	Comparison ₁	69.839±6.309	69.238±6.422	67.558±6.288	68.798±5.94	67.355±4.66	69.608±8.443	67.429±6.47	69.077±5.219	61.681±7.258	57.478±6.871
	Comparison ₂	69.434±15.443	69.14±15.786	68.76±15.184	67.843±15.447	67.721±17.138	67.645±16.934	67.534±17.682	66.804±17.62	66.186±15.261	65.334±14.453
	Comparison ₃	43.969±5.516	41.343±14.682	41.65±10.557	42.879±11.205	42.062±16.596	40.657±13.302	40.997±12.696	40.39±18.799	33.929±15.28	27.198±12.571

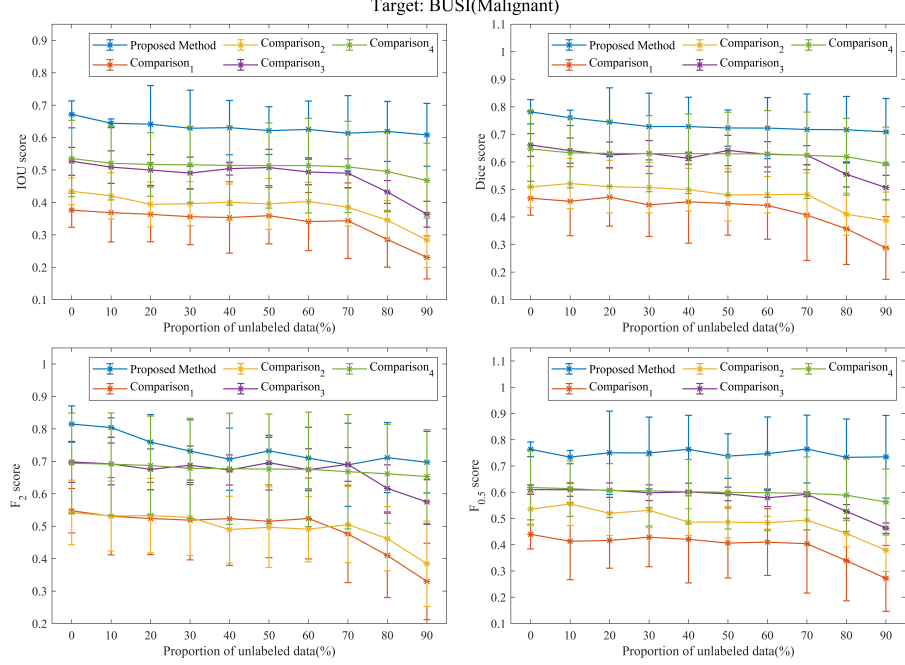


Figure 9: The method comparison experiment with BUSI (Malignant) as the target domain, and BUSI (Benign) and DDTI as the two source domains. The curves of the four indicators of IOU , $Dice\ score$, F_2 and $F_{0.5}$ as a function of the proportion of unlabeled data are plotted.

by a single source domain are always limited, multi-source transfer learning is adopted to supplement the available common features. Therefore, this paper needs to verify the effectiveness of adversarial transfer learning and multi-source learning respectively, as well as multi-source adversarial transfer learning, so the selected experiment types are shown in table 5.

3.6.1. BUSI(Benign) Ablation experiment Results and Analysis

Figure10 plots the trend of the test results in the table 6 in the proportion of unlabeled data from 0% to 90%. The multi-source adversarial transfer learning achieved the best results. Except for the adversarial transfer learning of BUSI Malignant as the source domain, the other experimental results are relatively close and not ideal. In addition, when using the multi-source adversarial transfer

Table 5: Experiments settings

	Name	Target	Source 1	Source 2	Method
Adversarial:	2 Sources	✓	✓	✓	ATL ^a
	Source 1	✓	✓		ATL
	Source 2	✓		✓	ATL
Ablation:	2 Sources	✓	✓	✓	MTL ^b
	Source 1	✓	✓		MTL
	Source 2	✓		✓	MTL
Only Target		✓			DL ^c

^a ATL = Adversarial Transfer Learning^b MTL = Multi-task Learning^c DL = Deep Learning

Table 6: BUSI(Benign) ablation experiment results

Target: BUSI(Benign)			The proportion of unlabeled data								
Score(%)	Experiment	0%	10%	20%	30%	40%	50%	60%	70%	80%	90%
IoU	2 Sources	66.197±5.239	63.725±5.832	65.545±6.714	63.68±7.845	61.718±0.76	61.986±2.343	59.749±3.998	59.216±7.682	52.359±10.259	46.45±9.653
	Adversarial: CT2US	60.9±4.367	59.386±8.085	57.574±8.791	55.808±8.522	55.198±9.812	53.548±11.906	53.289±5.716	52.654±7.172	51.252±5.856	43.914±14.226
	Malignant	60.766±3.009	61.109±4.809	59.299±6.232	59.884±4.831	57.004±5.233	56.484±6.479	57.281±9.46	53.816±0.656	41.43±6.25	33.782±4.118
	2 Sources	61.713±7.668	60.669±5.94	58.368±7.383	58.368±7.383	57.066±7.141	54.087±6.399	51.297±5.606	51.94±7.11	43.023±8.258	32.946±5.767
	Ablation: CT2US	61.524±9.213	59.918±8.133	60.541±7.359	56.406±7.748	58.179±11.427	54.224±7.5	51.037±6.199	48.505±6.852	38.609±7.062	30.407±6.697
	Malignant	59.571±4.337	59.872±7.471	59.555±4.771	58.028±6.15	57.43±9.812	53.95±10.013	52.334±8.863	46.902±10.273	32.808±12.033	32.444±3.832
	Only Target	58.04±6.394	55.809±7.7	56.863±11.512	52.98±1.232	50.426±9.927	49.471±6.288	49.81±8.704	47.962±8.954	40.707±11.326	32.487±11.031
	Without Independence	56.998±11.417	55.67±11.294	53.867±10.983	52.295±10.933	50.717±10.808	49.551±10.704	48.319±10.69	46.373±9.589	44.015±9.388	42.873±9.373
	2 Sources	76.361±5.16	74.044±5.86	74.893±5.53	73.212±7.127	72.99±0.663	72.743±1.347	71.055±2.694	69.868±6.797	63.931±10.241	57.94±10.535
	Adversarial: CT2US	72.029±4.178	69.617±7.424	68.426±8.388	66.193±8.141	65.927±10.667	64.686±13.259	63.71±7.218	63.125±7.438	63.783±4.518	48.892±17.473
Dice	Malignant	70.512±1.358	70.431±3.775	69.07±4.516	68.951±4.697	68.318±3.734	67.659±5.143	66.345±9.944	64.822±0.878	54.006±7.13	45.172±5.432
	2 Sources	71.045±7.403	70.628±5.748	68.554±7.636	68.554±7.636	67.754±7.277	65.671±6.056	62.817±5.248	62.944±6.246	55.066±9.22	44.392±5.493
	Ablation: CT2US	70.004±8.821	69.779±7.679	69.946±6.548	67.325±7.629	67.262±11.517	65.166±7.645	62.534±6.945	59.625±8.743	49.328±10.039	42.636±8.623
	Malignant	69.539±5.111	69.421±8.053	69.644±4.991	67.98±6.493	67.23±9.454	63.579±11.596	62.1±10.779	57.49±11.184	43.797±14.284	43.878±7.893
	Only Target	69.75±5.746	67.497±6.813	67.666±12.842	64.074±1.356	62.946±10.883	62.28±6.79	62.358±9.671	60.523±9.489	52.978±11.481	43.658±12.421
	Without Independence	65.721±13.133	64.551±12.131	62.124±11.833	60.851±11.592	59.178±11.481	57.049±11.201	55.804±11.003	52.817±10.84	48.984±10.754	47.851±10.514
	2 Sources	78.823±3.467	76.246±3.881	76.548±3.234	74.679±4.515	76.567±1.82	74.873±0.507	75.847±0.254	74.691±1.802	66.746±8.591	65.353±10.359
	Adversarial: CT2US	77.229±1.863	74.738±5.363	72.279±7.284	70.652±5.419	71.048±7.772	71.249±10.777	69.071±7.102	69.448±6.463	72.49±2.906	61.324±17.439
	Malignant	72.304±2.178	72.944±2.452	70.176±3.826	71.024±5.218	71.569±3.323	70.725±5.685	68.714±9.651	68.274±1.604	60.626±4.828	53.543±6.386
	2 Sources	73.627±6.436	73.672±4.704	72.854±7.039	72.854±7.039	70.891±7.153	69.567±4.571	68.204±5.587	67.489±4.343	61.042±9.755	53.22±4.318
F ₂	Ablation: CT2US	69.781±7.391	71.053±7.329	70.153±6.624	71.903±5.074	67.479±10.195	67.256±5.543	64.443±7.666	61.986±8.773	54.064±11.59	50.987±8.537
	Malignant	68.489±5.029	67.116±8.016	68.585±4.962	68.346±6.512	67.819±7.273	62.812±11.005	62.184±10.6	59.285±10.703	50.548±13.376	49.784±9.271
	Only Target	75.475±3.98	73.886±5.365	72.992±11.849	67.685±0.94	71.158±9.387	71.029±4.956	71.013±8.585	69.582±7.923	63.894±9.601	54.507±11.205
	Without Independence	70.217±8.743	65.878±7.486	65.535±7.002	65.507±6.598	65.449±6.404	65.348±6.372	64.65±4.727	64.556±3.547	60.881±3.313	59.739±2.993
	2 Sources	75.972±6.84	74.245±7.76	75.318±7.253	73.013±9.98	71.873±3.821	73.122±3.217	68.812±5.543	67.723±10.848	63.42±12.336	54.783±11.118
	Adversarial: CT2US	69.693±6.64	67.081±9.276	67.841±9.029	64.434±11.084	63.632±13.723	61.322±15.885	61.959±7.908	60.09±8.591	59.251±5.939	50.749±17.953
	Malignant	70.807±0.332	70.052±5.501	70.839±4.008	69.427±4.846	67.699±5.03	67.962±4.413	66.462±10.663	64.125±0.001	52.315±9.516	41.767±6.04
	2 Sources	70.369±8.475	69.636±7.013	66.675±8.133	66.675±8.133	66.587±7.776	64.265±8.373	60.2±4.746	61.036±8.014	53.37±9.423	41.174±6.578
	Ablation: CT2US	71.507±11.254	69.974±9.238	71.272±7.49	64.835±10.527	68.36±13.732	65.285±10.771	63.195±7.303	59.653±10.046	48.061±9.884	39.637±8.723
	Malignant	72.219±6.427	73.007±8.902	72.899±5.157	69.409±7.715	68.297±12.298	66.239±12.913	63.986±12.091	57.957±12.48	41.928±15.993	42.205±8.987
F _{0.5}	Only Target	67.453±6.851	64.152±7.759	65.232±13.101	63.128±3.133	58.635±11.935	57.549±9.102	57.538±11.054	55.545±11.279	47.949±12.71	39.903±14.107
	Without Independence	71.128±10.752	68.903±10.367	66.358±10.296	63.6±10.134	61.167±10.107	58.606±9.233	56.172±9.061	52.572±8.567	50.315±8.241	48.142±7.748

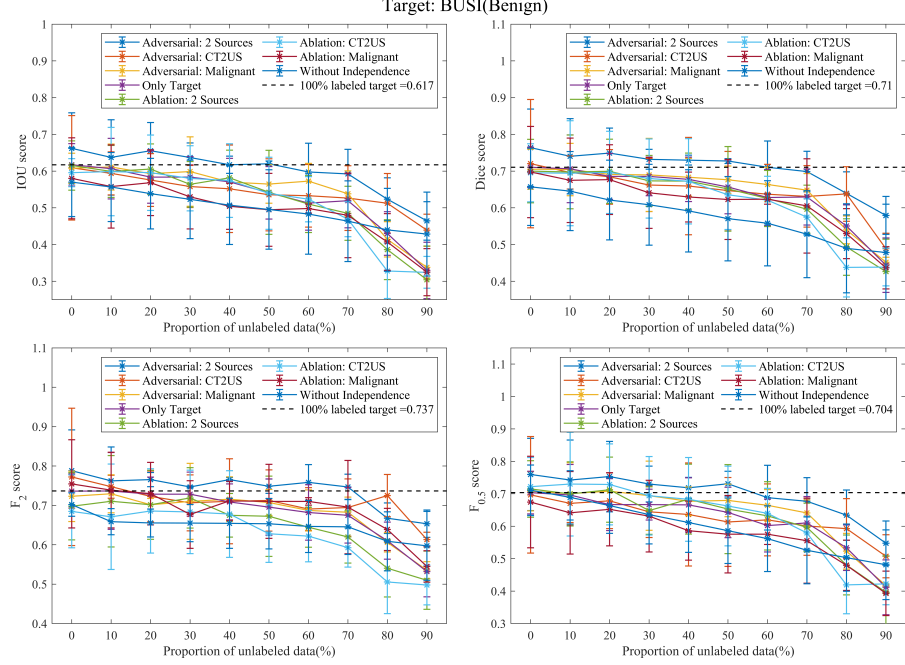


Figure 10: Ablation experiments with BUSI (Benign) as the target domain and BUSI (Malignant) and CT2US as the two source domains. The curves of the four indicators of IOU , $Dice$ score, F_2 and $F_{0.5}$ as a function of the proportion of unlabeled data are plotted.

learning method, only 40% of all the data can be used to achieve the target domain effect of using the 100% label under the same conditions. The effect of multi-source adversarial transfer learning is also better if the target domain has a larger proportion of labeled data. It can be seen that for deep learning that only uses the target domain, when the proportion of labeled data is insufficient, the performance is seriously degraded, overfitting occurs, and the performance on the test set is not good enough. The effect of adversarial transfer learning using two source domains is significantly better than using only the target domain and multi-task learning ablation experiments, indicating that the common features that can be extracted through the adversarial structure are more conducive to the improvement of the target domain task. The comparative experiments of adversarial transfer learning with two separate source domains are weaker than

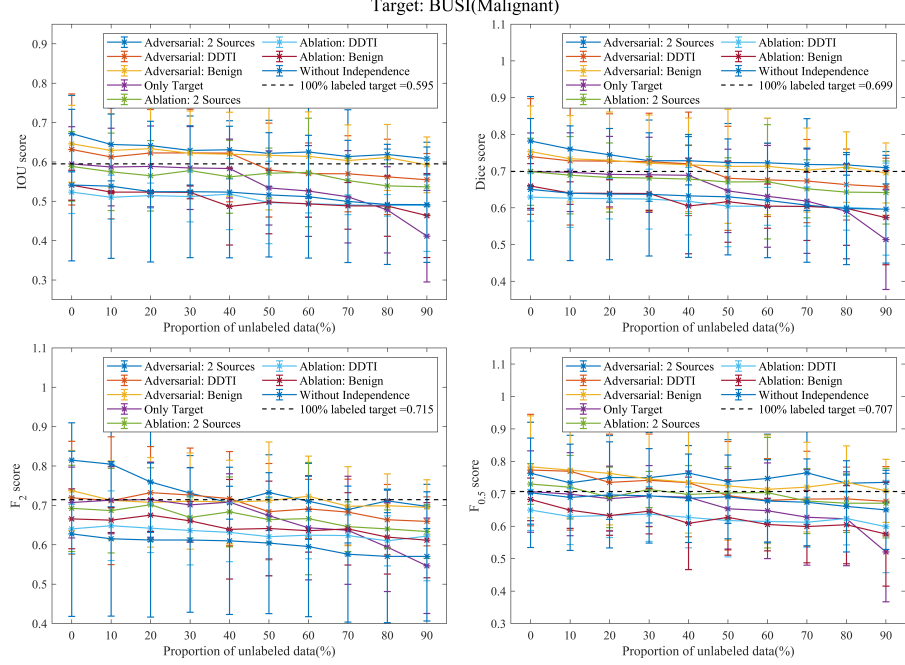


Figure 11: Ablation experiments with BUSI (Malignant) as the target domain and BUSI (Benign) and DDTI as the two source domains. The curves of the four indicators of IOU , $Dice$ score, F_2 and $F_{0.5}$ as a function of the proportion of unlabeled data are plotted.

multi-source adversarial transfer learning at all times, and it can be considered that multiple source domains provide more information than a single source domain. After deleting the multi-source domain independent policy, you can see a significant drop in performance. We think this is because after removing this strategy, there is no way to guarantee that the data from the target domain in each sub-batch is completely consistent, resulting in poor fusion effect.

3.6.2. BUSI(Malignant) Ablation experiment Results and Analysis

BUSI(Malignant)'s specific experimental results are shown in Table 7. Figure 11 plots the trend of the test results of IOU , $Dice$, F_2 and $F_{0.5}$ for all experiments in table 5 as the proportion of unlabeled data increases. Overall, the four indicators of the BUSI(Malignant) experiment are overall higher

Table 7: BUSI(Malignant) ablation experiment results

Target: BUSI(Malignant)		Proportion of unlabeled data									
Score(%)	Experiment	0%	10%	20%	30%	40%	50%	60%	70%	80%	90%
IoU	Adversarial: 2 Sources	DDTI	67.177±1.140	64.422±1.358	64.154±1.891	62.906±1.746	63.08±1.387	62.168±1.378	62.521±1.765	61.352±1.588	61.007±1.248
		Benign	64.165±6.695	61.251±9.591	62.271±9.665	62.262±7.773	62.236±11.934	57.941±12.381	57.038±11.113	56.991±11.051	56.193±15.708
	Benign	DDTI	64.598±7.075	62.913±8.386	63.384±9.065	62.18±11.349	61.96±13.866	61.675±10.65	61.39±10.747	60.34±10.632	61.123±9.346
		2 Sources	59.506±11.618	58.708±10.952	58.857±11.732	58.464±11.545	58.321±9.413	53.39±7.493	52.599±10.53	51.145±10.278	47.825±9.801
	Ablation: 2 Sources	DDTI	58.856±7.060	57.481±5.611	56.441±5.674	57.791±13.778	56.322±6.382	57.142±8.27	57.331±5.102	55.349±8.938	53.989±9.847
		Benign	52.313±11.688	51.021±7.728	51.455±5.487	51.203±2.351	51.835±10.453	49.698±9.041	49.402±6.443	49.094±3.154	48.962±5.615
	Only Target	DDTI	54.097±10.653	52.338±7.672	52.343±5.942	52.267±3.344	48.682±8.079	49.807±9.781	49.328±1.63	48.833±0.349	48.787±0.282
		2 Sources	54.112±14.193	53.83±14.282	52.45±14.482	52.443±14.830	52.344±15.467	51.632±15.842	51.156±16.09	49.974±16.464	49.196±17.36
	Without Independence	DDTI	78.194±4.405	75.989±2.795	74.431±12.49	72.927±12.112	72.862±10.601	72.337±8.973	72.262±11.094	71.796±12.876	71.676±12.112
		2 Sources	78.194±4.405	75.989±2.795	74.431±12.49	72.927±12.112	72.862±10.601	72.337±8.973	72.262±11.094	71.796±12.876	71.676±12.112
Dice	Adversarial: 2 Sources	DDTI	73.963±7.768	72.779±9.466	72.698±11.326	72.552±9.944	71.989±14.152	68.945±14.082	67.622±13.183	67.286±12.915	66.333±17.451
		Benign	75.304±8.156	73.343±9.607	72.936±11.44	72.132±13.136	71.73±15.526	71.285±12.687	71.304±13.146	70.271±13.168	71.092±11.758
	Benign	DDTI	69.903±13.569	69.702±12.931	69.134±14.195	68.993±13.866	68.847±11.36	64.62±8.125	63.132±10.22	61.819±10.293	59.057±10.702
		2 Sources	69.83±8.58	68.875±6.341	68.297±7.901	68.108±15.562	67.835±6.50	67.02±9.312	67.098±5.851	65.201±9.399	64.287±10.539
	Ablation: 2 Sources	DDTI	62.912±12.537	62.617±6.179	62.485±5.311	62.376±5.162	61.8±11.04	60.477±5.169	60.414±8.157	60.34±5.499	60.107±7.955
		Benign	65.937±12.825	64.012±10.053	63.93±9.262	63.891±6.013	60.512±11.051	61.668±13.015	60.463±4.622	60.371±3.714	59.854±3.065
	Only Target	DDTI	59.629±14.656	59.803±15.237	60.72±15.526	62.041±15.551	62.987±15.789	63.247±16.719	63.667±16.768	63.736±17.875	63.98±18.335
		2 Sources	59.629±14.656	59.803±15.237	60.72±15.526	62.041±15.551	62.987±15.789	63.247±16.719	63.667±16.768	63.736±17.875	63.98±18.335
	Without Independence	DDTI	81.505±5.895	80.462±2.995	79.992±2.46	79.144±9.444	70.975±9.604	73.262±1.9	71.033±7.61	68.58±12.816	71.177±10.811
		2 Sources	81.505±5.895	80.462±2.995	79.992±2.46	79.144±9.444	70.975±9.604	73.262±1.9	71.033±7.61	68.58±12.816	71.177±10.811
F ₂	Adversarial: 2 Sources	DDTI	71.949±6.222	71.189±8.935	73.234±9.371	72.446±7.483	71.725±12.234	68.421±11.957	69.125±11.9	68.29±11.727	66.376±16.237
		Benign	73.764±6.965	71.308±8.051	70.78±10.024	71.09±10.217	70.833±14.926	71.185±10.608	72.305±12.221	69.793±11.379	69.939±9.999
	Benign	DDTI	70.719±12.12	71.329±11.28	71.459±13.714	70.131±13.234	70.84±10.949	67.377±7.209	64.324±9.486	63.668±9.549	59.399±8.52
		2 Sources	69.235±6.791	68.682±4.824	70.184±5.314	66.932±14.207	68.366±5.769	66.386±8.867	66.647±5.196	64.607±5.356	64.028±10.739
	Ablation: 2 Sources	DDTI	64.036±11.313	64.855±6.353	64.219±5.206	63.637±6.001	63.162±9.949	62.07±7.453	62.453±8.748	62.353±6.171	61.01±8.854
		Benign	66.578±9.54	66.268±9.403	67.529±9.179	66.086±5.426	63.938±12.015	64.142±12.636	63.58±4.94	64.044±4.116	61.968±3.157
	Only Target	DDTI	57.057±10.401	57.036±16.82	57.821±17.266	59.569±17.833	60.425±17.899	60.998±18.684	61.224±18.336	61.206±19.556	61.512±19.635
		2 Sources	57.057±10.401	57.036±16.82	57.821±17.266	59.569±17.833	60.425±17.899	60.998±18.684	61.224±18.336	61.206±19.556	61.512±19.635
	Without Independence	DDTI	76.354±2.787	73.405±2.529	75.043±15.874	74.982±15.667	76.376±12.921	73.777±8.488	74.74±13.963	76.409±12.301	75.297±14.922
		2 Sources	76.354±2.787	73.405±2.529	75.043±15.874	74.982±15.667	76.376±12.921	73.777±8.488	74.74±13.963	76.409±12.301	75.297±14.922
F _{0.5}	Adversarial: 2 Sources	DDTI	77.327±10.665	76.545±9.795	73.529±14.75	74.172±12.848	73.441±16.719	69.463±16.68	68.014±14.24	68.386±14.854	68.444±18.15
		Benign	78.325±9.723	77.301±11.218	76.299±13.836	74.566±16.745	73.579±16.757	72.466±15.702	71.407±14.8	72.065±15.868	73.582±14.682
	Benign	DDTI	70.71±15.348	69.882±14.456	68.524±14.781	69.324±14.773	68.949±12.424	65.375±8.094	64.771±9.391	62.777±10.024	62.308±12.791
		2 Sources	70.71±15.348	69.882±14.456	68.524±14.781	69.324±14.773	68.949±12.424	65.375±8.094	64.771±9.391	62.777±10.024	62.308±12.791
	Ablation: 2 Sources	DDTI	73.022±10.728	72.038±9.067	68.898±10.688	71.357±17.074	69.806±8.078	70.308±8.916	70.374±5.567	67.772±9.338	67.122±9.804
		Benign	65.024±14.173	63.009±8.113	63.35±7.701	63.784±6.036	62.726±11.198	61.763±9.379	61.49±8.445	61.248±6.827	59.446±6.324
	Only Target	DDTI	68.278±12.066	64.945±12.027	63.278±11.149	64.662±8.122	60.889±11.627	62.717±14.265	60.535±7.04	59.805±6.049	60.463±5.603
		2 Sources	68.278±12.066	64.945±12.027	63.278±11.149	64.662±8.122	60.889±11.627	62.717±14.265	60.535±7.04	59.805±6.049	60.463±5.603
	Without Independence	DDTI	65.047±12.224	66.136±14.06	67.389±13.377	67.799±12.699	69.056±12.895	68.633±13.648	69.361±14.561	69.687±16.365	68.924±16.361
		2 Sources	65.047±12.224	66.136±14.06	67.389±13.377	67.799±12.699	69.056±12.895	68.633±13.648	69.361±14.561	69.687±16.365	68.924±16.361

than those of BUSI(Benign). It can be seen that in the process of increasing the proportion of unlabeled data from 10% to 90%, the effect of adversarial transfer learning using two source domains is significantly better than other experimental results. It shows that the multi-source adversarial transfer learning applied to the BUSI(Malignant) dataset shows better performance. The multi-source adversarial transfer learning strategy still performs the best. The BUSI(Malignant) is better than the BUSI(Benign) experiment, the multi-source adversarial transfer learning metric decreases less as the proportion of labeled samples decreases. Because these two labeled source domains can provide more comprehensive deep features, high accuracy can be achieved without too many labels in the segmented part. When using only BUSI(Benign) as the source domain, it can be seen that the accuracy is close but slightly lower than multi-source adversarial transfer learning. It shows that although the source domain can provide most of the knowledge information of the target domain segmentation task, it does not yet contain all the knowledge required by the target domain; When only DDTI is used as the source domain, and the unlabeled ratio is about 40%-50%, the performance begins to drop significantly, and more target domain labels are needed to screen out features that are more beneficial to the target task through confrontation; For deep learning that only uses the target domain, the performance drops significantly at about 40%-50% and 80%-90%.

This is due to overfitting due to insufficient labeled training data. The effect of adding an adversarial structure is also significantly better than that of multi-task learning without an adversarial structure (including one target domain and two source domains for a total of three tasks). It can be considered that the common features of adversarial structure extraction are more conducive to the improvement of target domain tasks. In addition, it can also be seen that the comparative experiments of adversarial transfer learning of two single source domains are weaker than multi-source adversarial transfer learning at all times. It can be considered that the information provided by multiple source domains is more than that of a single-source domain. The overall effect of ablation experiments is not as good as that of adversarial transfer learning, and even some experimental performances are not as good as the performance of using only the target domain data, indicating that adding domain classifiers is beneficial to extract common features that improve the performance of target domain tasks.

3.7. Parameter ablation experiment results and analysis

We also refer to the work [17] to explore some key parameters. For the parameters α and λ of the equation (16), the influence of different weight coefficients on the performance of the model is studied, and an ablation experiment is designed. We believe that the parameter weights α and λ can be easily set according to specific needs in practical application scenarios. Specifically, we randomly prepare several sets of weights for testing on two target domain datasets.

3.7.1. BUSI(Benign) parameter ablation experiment results and analysis

We tested the performance metrics *IOU*, *Dice score*, F_2 and $F_{0.5}$ on the BUSI(Benign) dataset with different proportions of unlabeled data. The results are shown in the table 8. Figure 12 plots the trend of the proportion of unlabeled data for all experiments in the table 8 from 0% to 90%. It can be seen that among the four indicators, #1 and #2 have the best performance.

Specifically, #1 has better performance when there are more labeled data and less unlabeled data. When the labeled data is less and the unlabeled data is more, the performance of #2 is better. It can be observed that the performance of #4 begins to drop significantly when the unlabeled data reaches 50%. We think this is because the parameter λ used for confrontation is too small. The difference is that although #6 performs better when there are fewer tags, its performance is generally not as good as #1 and #2. We believe this is due to the fact that the split predictors are underweighted. BUSI(Benign) parameter ablation experiments show that, in general, performance is better with different scales of labeled data when the weights are within a reasonable range of values close to each other. If the weight gap is too large, the error will increase accordingly when it is largely biased towards certain values.

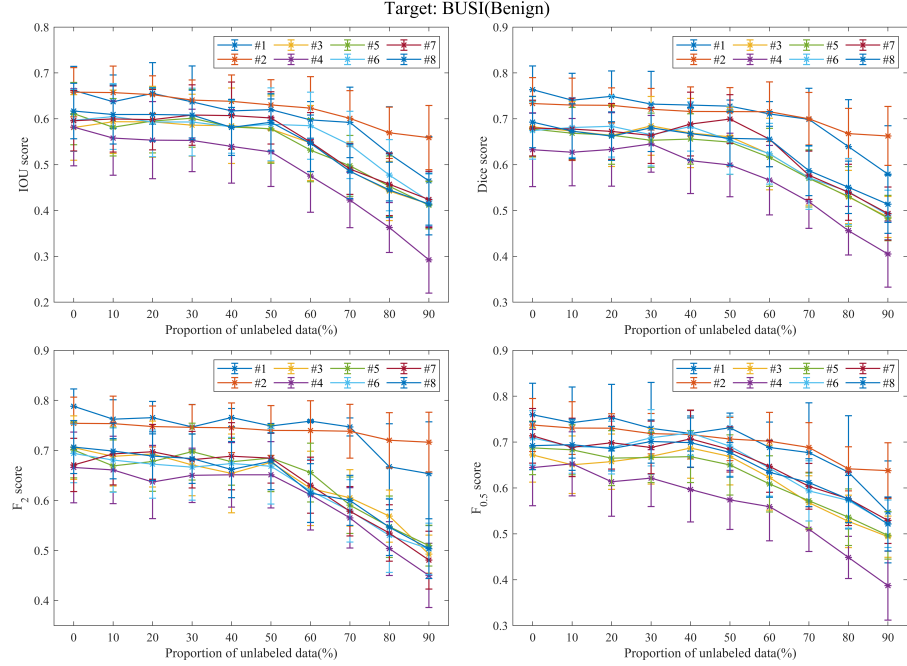


Figure 12: Parametric ablation experiments using BUSI(Benign) as the target domain, and BUSI(Malignant) and CT2US as the two source domains. The curves of the four indicators of IOU , $Dice\ score$, F_2 and $F_{0.5}$ as a function of the proportion of unlabeled data are plotted.

Table 8: BUSI(Benign) parameter ablation experiment results

Target: BUSI(Benign)		Group		α	λ	0%	10%	20%	30%	Proportion of unlabeled data									
Score(%)										40%	50%	60%	70%	80%	90%				
IoU	#1	1	1	66.197 \pm 5.339	63.735 \pm 5.832	63.545 \pm 6.714	63.682 \pm 7.845	63.718 \pm 6.76	63.596 \pm 5.343	59.740 \pm 3.998	59.216 \pm 7.682	52.359 \pm 10.359	46.45 \pm 5.483						
	#2	2	3	65.79 \pm 5.383	65.719 \pm 5.785	65.267 \pm 4.098	64.077 \pm 4.384	63.821 \pm 5.749	63.031 \pm 5.486	62.331 \pm 8.865	60.076 \pm 6.057	56.94 \pm 5.592	55.888 \pm 7.902						
	#3	1	4	58.098 \pm 7.153	59.359 \pm 6.911	59.329 \pm 7.732	58.595 \pm 6.752	58.486 \pm 8.226	57.773 \pm 7.217	54.722 \pm 8.185	48.599 \pm 6.34	44.254 \pm 6.459	41.404 \pm 4.954						
	#4	3	1	58.174 \pm 8.429	55.787 \pm 8.093	55.336 \pm 8.398	55.284 \pm 8.803	53.974 \pm 8.009	52.775 \pm 7.549	47.51 \pm 7.907	42.267 \pm 6.022	36.283 \pm 5.456	29.235 \pm 7.246						
	#5	5	3	61.12 \pm 6.789	58.161 \pm 6.255	59.512 \pm 6.952	60.107 \pm 6.314	58.199 \pm 5.691	57.827 \pm 7.537	53.153 \pm 6.873	49.734 \pm 6.649	45.276 \pm 6.597	41.141 \pm 5.162						
	#6	1	5	59.66 \pm 6.784	60.405 \pm 7.19	59.288 \pm 7.533	59.301 \pm 7.389	58.242 \pm 6.76	58.784 \pm 7.954	58.488 \pm 7.308	54.308 \pm 7.338	47.704 \pm 7.772	42.107 \pm 5.36						
	#7	5	2	59.575 \pm 6.594	59.954 \pm 7.215	59.804 \pm 6.587	60.812 \pm 6.596	60.689 \pm 7.321	60.19 \pm 5.704	54.931 \pm 6.414	49.045 \pm 5.546	45.711 \pm 6.822	42.394 \pm 6.153						
	#8	2	1	61.683 \pm 6.043	60.929 \pm 6.435	60.926 \pm 5.808	60.826 \pm 5.392	58.116 \pm 6.112	59.25 \pm 6.234	54.65 \pm 6.171	48.528 \pm 5.942	44.889 \pm 6.032	41.406 \pm 6.733						
$Dice$	#1	1	1	76.361 \pm 5.16	74.044 \pm 5.86	74.893 \pm 5.53	73.212 \pm 7.127	72.99 \pm 6.663	72.743 \pm 1.347	71.055 \pm 2.694	69.868 \pm 2.797	63.931 \pm 10.241	57.94 \pm 10.535						
	#2	2	3	73.337 \pm 5.639	72.997 \pm 5.855	72.917 \pm 3.824	72.082 \pm 4.538	71.597 \pm 5.361	71.571 \pm 5.224	71.539 \pm 6.517	70.008 \pm 5.741	66.772 \pm 5.494	66.256 \pm 6.432						
	#3	1	4	68.238 \pm 6.589	67.317 \pm 6.434	66.365 \pm 6.78	68.467 \pm 6.41	66.894 \pm 7.54	66.066 \pm 6.44	62.315 \pm 7.794	57.189 \pm 6.039	52.95 \pm 5.806	48.581 \pm 4.482						
	#4	3	1	63.265 \pm 8.044	62.721 \pm 7.335	63.313 \pm 6.025	64.532 \pm 6.182	60.859 \pm 7.172	59.916 \pm 6.93	56.619 \pm 7.568	51.925 \pm 5.333	45.584 \pm 5.299	40.506 \pm 7.215						
	#5	5	3	67.745 \pm 6.035	66.85 \pm 5.64	66.433 \pm 6.343	65.321 \pm 5.916	65.596 \pm 5.488	64.91 \pm 7.029	61.593 \pm 6.32	57.6 \pm 2.37	53.064 \pm 6.512	48.353 \pm 4.953						
	#6	1	5	67.439 \pm 6.248	68.088 \pm 6.528	68.362 \pm 6.706	66.519 \pm 6.815	68.318 \pm 5.372	65.344 \pm 7.451	62.378 \pm 6.63	57.133 \pm 6.88	54.123 \pm 7.217	49.041 \pm 5.387						
	#7	5	2	67.964 \pm 6.079	67.748 \pm 6.754	67.248 \pm 6.083	66.363 \pm 6.096	68.845 \pm 6.948	69.946 \pm 5.314	65.55 \pm 5.999	57.699 \pm 5.261	53.958 \pm 6.109	49.334 \pm 5.794						
	#8	2	1	69.283 \pm 5.613	67.302 \pm 5.959	66.221 \pm 5.292	68.035 \pm 5.185	66.766 \pm 5.754	65.735 \pm 5.905	65.558 \pm 6.014	58.696 \pm 5.466	55.068 \pm 5.719	51.371 \pm 6.344						
F_2	#1	1	1	74.823 \pm 5.467	74.246 \pm 5.881	74.348 \pm 5.234	74.679 \pm 4.515	74.507 \pm 1.142	74.873 \pm 2.507	73.847 \pm 2.234	74.691 \pm 1.802	66.146 \pm 3.591	63.335 \pm 10.359						
	#2	2	3	75.41 \pm 5.238	75.353 \pm 5.5	74.786 \pm 4.081	74.61 \pm 4.554	74.515 \pm 4.96	73.993 \pm 4.979	73.067 \pm 5.864	73.828 \pm 5.381	72.023 \pm 5.522	71.657 \pm 5.96						
	#3	1	4	70.556 \pm 6.342	68.808 \pm 5.91	69.277 \pm 6.583	67.094 \pm 6.135	65.42 \pm 7.872	67.625 \pm 5.87	62.412 \pm 7.422	60.525 \pm 5.635	56.87 \pm 5.207	49.282 \pm 3.799						
	#4	3	1	66.612 \pm 7.068	66.095 \pm 6.736	63.697 \pm 7.317	65.015 \pm 4.32	65.12 \pm 6.437	65.134 \pm 6.632	61.101 \pm 6.993	56.524 \pm 6.036	50.398 \pm 5.381	45.025 \pm 6.412						
	#5	5	3	70.085 \pm 5.566	66.91 \pm 5.187	67.791 \pm 5.943	69.754 \pm 5.679	67.725 \pm 4.659	68.474 \pm 6.671	65.566 \pm 5.873	59.058 \pm 5.643	54.765 \pm 6.139	50.97 \pm 4.08						
	#6	1	5	69.401 \pm 5.836	68.064 \pm 6.437	67.274 \pm 6.317	66.06 \pm 6.6	67.366 \pm 5.25	66.85 \pm 7.07	61.927 \pm 6.306	57.931 \pm 6.243	53.029 \pm 7.402	50.321 \pm 5.144						
	#7	5	2	67.102 \pm 5.318	69.311 \pm 6.201	69.724 \pm 5.469	68.155 \pm 5.653	68.848 \pm 6.698	68.446 \pm 4.977	63.042 \pm 5.599	57.845 \pm 4.992	53.507 \pm 5.649	48.086 \pm 5.774						
	#8	2	1	70.669 \pm 5.295	69.88 \pm 5.562	68.868 \pm 4.864	68.363 \pm 4.941	66.183 \pm 5.609	67.835 \pm 5.681	61.475 \pm 5.878	60.018 \pm 4.996	54.652 \pm 5.635	50.373 \pm 5.977						
$F0.5$	#1	1	1	75.972 \pm 6.984	74.545 \pm 7.76	75.318 \pm 7.253	73.013 \pm 9.08	71.873 \pm 8.821	73.12 \pm 3.217	68.812 \pm 5.543	67.723 \pm 10.848	63.42 \pm 12.336	54.783 \pm 11.118						
	#2	2	3	73.721 \pm 5.784	73.063 \pm 5.755	73.024 \pm 5.152	71.843 \pm 4.397	71.648 \pm 5.333	70.674 \pm 4.726	70.18 \pm 6.3	68.838 \pm 5.409	64.186 \pm 4.807	63.783 \pm 6.078						
	#3	1	4	67.183 \pm 5.909	65.056 \pm 6.275	65.729 \pm 6.028	66.88 \pm 6.043	68.702 \pm 6.585	66.862 \pm 6.192	62.258 \pm 7.106	56.788 \pm 5.874	52.711 \pm 5.713	49.377 \pm 4.499						
	#4	3	1	64.44 \pm 8.312	65.263 \pm 8.8	63.357 \pm 7.515	62.145 \pm 6.209	59.972 \pm 7.07	57.401 \pm 6.445	55.915 \pm 7.45	51.019 \pm 4.866	44.857 \pm 4.594	38.7 \pm 5.51						
	#5	5	3	68.735 \pm 5.841	68.306 \pm 5.485	66.505 \pm 5.989	66.636 \pm 5.451	66.841 \pm 5.676	65.014 \pm 6.566	60.892 \pm 6.12	57.211 \pm 6.056	53.631 \pm 6.171	49.671 \pm 5.181						
	#6	1	5	70.906 \pm 5.924	69.043 \pm 6.838	68.792 \pm 5.742	70.937 \pm 6.144	72.009 \pm 4.862	69.108 \pm 6.56	64.32 \pm 6.104	59.373 \pm 6.561	57.291 \pm 6.039	52.194 \pm 5.168						
	#7	5	2	71.361 \pm 5.956	68.851 \pm 6.359	69.863 \pm 5.753	68.842 \pm 5.719	70.698 \pm 6.238	68.377 \pm 4.915	64.716 \pm 5.659	60.365 \pm 4.999	57.634 \pm 5.828	52.919 \pm 5.019						
	#8	2	1	69.206 \pm 5.21	69.441 \pm 5.593	68.571 \pm 4.863	70.121 \pm 4.713	69.889 \pm 5.37	67.734 \pm 5.382	63.414 \pm 5.433	61.169 \pm 5.214	57.58 \pm 5.136	52.147 \pm 5.885						

3.7.2. BUSI(Malignant) parameter ablation experiment results and analysis

Similar to the parameter ablation experiment of BUSI (Benign), the figure 13 draws the trend of the test results in the table 9. Like BUSI(Benign), #1 and #2 perform best. It is worth noting that #2 has very limited performance degradation as the number of labels decreases. We believe that under the condition that the weight of the segmentation predictor is not too small, the coefficient of the corresponding item of the domain discriminator in the loss function can be appropriately increased within a certain range to achieve better performance with fewer labels.

In summary, multi-source adversarial transfer learning can increase the generalization ability of the model through the strategy of transfer learning; Through the method of adversarial transfer learning, some common features that can improve the performance of the target domain can be extracted from some source domains that have a certain appearance gap with the target domain; If the key features provided by a source domain that are beneficial to the target domain task are not sufficient, the missing key features can be filled by multiple source domains with different similarities. Through two comparative experiments, it can be seen that the proposed multi-source adversarial transfer learning method has better potential when the similarity between the source domain ultrasound

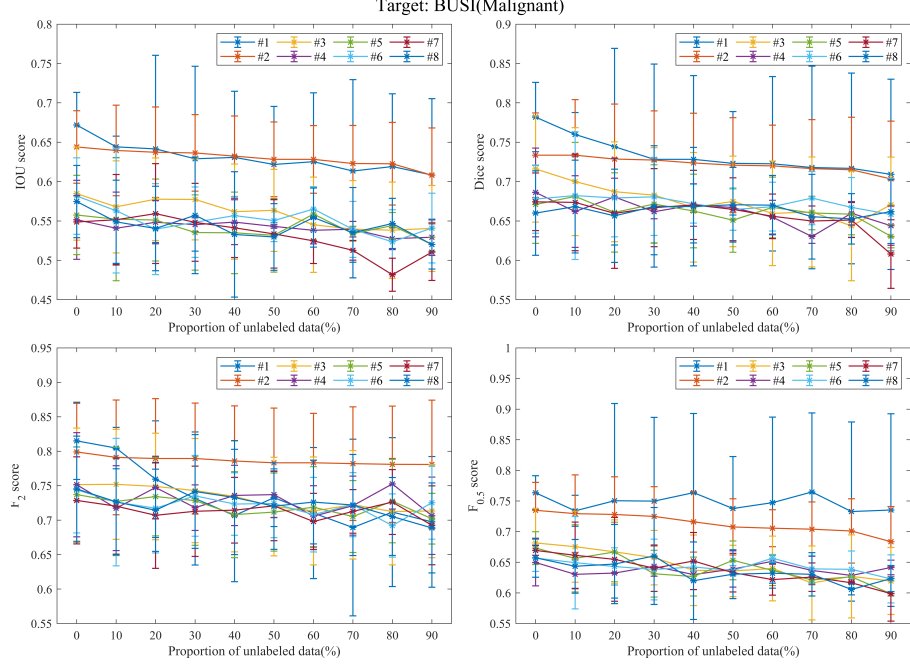


Figure 13: Parametric ablation experiments using BUSI(Malignant) as the target domain, and BUSI(Benign) and DDTI as the two source domains. The curves of the four indicators of IOU , $Dice$ score, F_2 and $F_{0.5}$ as a function of the proportion of unlabeled data are plotted.

image and the target domain ultrasound image is insufficient, and only some local features are similar. The ablation experiments prove that in the face of such a scene with insufficient global similarity but local similarity, the proposed multi-source adversarial transfer learning can extract more source domains to assist target domain learning to obtain better performance knowledge. Can handle this scenario better. Through parameter ablation experiments, we found that the weight of the segmentation predictor can be appropriately increased when there is more labeled data, and the weight of the domain classifier should be appropriately increased when the labeled data is insufficient. The weights of both are very important, and a set of relatively close parameters α and λ can be selected, because unbalanced parameters will lead to a decrease in the performance of the proposed method.

Table 9: BUSI(Malignant) parameter ablation experiment results

Target: BUSI(Malignant)				Proportion of unlabeled data									
Score(%)	Group	α	λ	0%	10%	20%	30%	40%	50%	60%	70%	80%	90%
I_{oU}	#1	1	1	67.177±4.149	64.422±1.358	64.154±11.893	62.908±11.746	63.08±8.387	62.168±7.378	62.521±8.705	61.352±11.598	61.907±9.248	60.841±9.704
	#2	2	3	64.394±4.609	63.955±5.757	63.727±5.748	63.64±4.861	63.227±5.106	62.83±4.748	62.836±4.297	62.306±4.827	62.27±5.243	60.815±5.999
	#3	1	4	58.478±5.919	56.787±5.854	57.757±5.245	57.735±5.132	56.183±6.038	56.346±5.207	54.524±6.054	53.952±6.183	53.824±6.116	54.053±5.456
	#4	3	1	55.148±5.021	54.071±4.598	54.839±2.742	54.531±0.870	54.847±2.847	54.307±0.21	53.814±1.731	53.953±0.989	52.749±1.395	52.921±2.311
	#5	5	3	55.761±5.037	55.217±7.807	55.117±5.204	53.533±4.776	53.486±5.174	53.177±4.077	55.874±3.298	53.382±0.938	54.414±1.662	52.014±0.934
	#6	1	5	58.161±4.854	56.297±7.908	53.956±5.778	54.839±4.474	55.974±2.428	55.04±2.657	56.503±2.847	53.927±3.563	52.353±4.074	54.092±4.433
	#7	5	2	54.879±3.33	55.16±5.752	55.937±6.335	54.822±4.953	54.125±3.768	53.358±4.348	52.478±2.882	51.269±1.255	48.16±2.097	51.042±3.603
	#8	2	1	57.467±4.592	54.891±5.288	54.04±5.362	55.709±7.405	53.29±7.958	52.97±4.233	55.430±3.757	53.516±5.738	54.68±3.187	52.009±3.126
$Dice$	#1	1	1	78.194±4.405	75.988±2.793	74.431±12.49	72.827±12.112	72.83±10.631	72.317±6.573	72.262±11.084	71.795±12.875	71.676±12.112	70.921±12.085
	#2	2	3	73.355±5.373	73.354±7.054	72.859±6.995	72.735±6.255	72.77±6.316	72.087±6.037	72.003±5.164	71.64±6.24	71.511±6.668	70.334±7.351
	#3	1	4	71.607±5.751	70±5.832	68.708±6.355	68.274±5.941	66.727±6.961	67.483±5.746	65.968±6.642	66.149±5.987	64.372±6.957	67.602±5.046
	#4	3	1	68.622±5.642	66.192±4.55	68.044±2.376	66.17±0.888	67.024±2.699	66.711±0.203	65.483±2.145	63.019±0.862	65.981±1.49	64.4±2.5
	#5	5	3	67.099±4.952	68.113±6.875	66.079±5.045	67.154±4.982	66.262±4.669	65.097±4.079	66.721±3.855	66.014±2.126	65.858±2.605	63.045±1.465
	#6	1	5	67.776±4.336	68.226±8.113	67.919±4.937	68.072±4.913	67.176±2.452	66.443±2.632	66.818±3.095	67.9±3.384	66.731±3.785	65.824±4.59
	#7	5	2	67.436±3.661	67.36±6.141	65.971±6.995	66.689±4.951	67.042±4.391	66.477±3.995	65.585±2.832	64.999±1.907	65.118±2.22	60.798±4.355
	#8	2	1	65.996±5.358	66.836±5.892	65.655±5.917	66.847±7.715	66.822±7.523	67.09±5.476	67.009±3.764	65.546±5.381	65.205±3.203	66.187±4.053
P_2	#1	1	1	81.505±5.605	80.462±5.095	75.952±8.46	73.144±2.648	70.675±9.694	73.26±2.139	71.03±5.51	68.938±5.816	71.17±0.811	69.733±9.483
	#2	2	3	79.89±7.065	79.114±8.326	78.946±8.699	78.944±8.057	78.579±8.099	78.334±7.927	78.32±7.178	78.208±8.246	78.112±8.431	78.078±9.328
	#3	1	4	75.169±8.188	75.203±7.979	74.892±7.73	74.29±7.554	73.449±8.045	71.97±7.153	71.336±7.83	72.23±7.867	71.245±7.731	71.33±6.761
	#4	3	1	75.133±7.556	71.745±6.154	74.733±4.545	71.815±3.297	73.593±4.369	73.714±3.347	70.557±4.45	72.108±4.275	75.265±3.654	70.643±5.611
	#5	5	3	73.713±6.899	72.72±7.86	73.42±5.691	72.849±6.49	70.802±6.237	71.171±5.671	71.883±5.871	70.531±5.22	72.769±6.056	70.212±3.66
	#6	1	5	74.408±6.264	72.618±6.255	71.741±6.496	73.524±5.868	72.34±4.527	72.427±4.973	70.799±5.419	72.249±4.652	69.225±4.585	72.544±5.31
	#7	5	2	72.871±6.315	72.035±6.961	70.7±7.694	71.295±6.556	71.443±4.765	72.077±5.059	69.81±4.086	71.269±3.17	72.624±4.706	69.256±5.724
	#8	2	1	74.532±7.671	72.65±7.487	71.434±5.969	74.159±8.257	73.279±8.279	72.044±6.275	72.624±6.078	72.198±7.339	70.528±5.654	68.876±6.524
$P_{0.5}$	#1	1	1	76.354±2.787	73.403±2.529	75.043±15.874	74.982±13.667	76.376±12.921	73.777±8.488	74.74±13.963	76.469±12.901	73.277±14.622	73.53±15.722
	#2	2	3	73.992±4.562	72.935±6.324	72.807±6.154	72.406±4.841	71.594±4.928	70.77±4.591	70.503±3.01	70.409±4.435	70.12±3.252	68.563±5.733
	#3	1	4	68.166±5.604	67.546±5.805	66.7±5.218	65.754±4.435	63.691±5.764	63.584±4.201	63.981±5.286	61.622±6.03	62.693±6.783	61.954±5.463
	#4	3	1	64.973±3.814	63.032±2.356	63.24±0.067	64.343±1.623	62.983±1.015	63.904±2.953	65.164±0.352	63.662±2.314	62.448±0.726	64.152±1.188
	#5	5	3	67.319±2.665	65.633±5.487	66.079±4.869	63.135±3.826	62.607±3.169	65.321±3.166	63.663±2.461	62.131±0.639	62.623±0.127	59.87±0.365
	#6	1	5	65.688±2.171	64.932±7.535	64.308±3.052	63.817±4.965	64.24±0.629	63.656±0.835	65.666±0.618	63.925±2.195	63.859±2.985	62.291±3.919
	#7	5	2	66.932±0.789	66.15±5.492	65.491±6.844	64.032±3.78	65.201±4.667	63.301±3.151	62.165±2.522	62.577±2.23	61.693±0.138	59.76±4.487
	#8	2	1	65.728±3.169	64.35±4.387	64.705±6.463	66.02±7.911	61.986±6.327	63.051±3.992	63.213±1.625	63.037±3.536	60.555±0.882	62.324±2.13

4. CONCLUSION

We propose a novel multi-source adversarial transfer learning network for the task of source-domain ultrasound image segmentation with limited similarity to the target domain. Specifically, through the strategy of adversarial transfer learning, general deep features beneficial to target domain tasks are adaptively extracted from different source domains, respectively, and the unlabeled target domain data is maximized. By leveraging knowledge from multiple source domains to supplement key features lacking in a single source domain and target domain due to lack of similarity, a multi-source transfer learning strategy is used to optimize task performance as much as possible. The segmentation results on three organ datasets confirm the good transfer learning ability of multi-source adversarial transfer learning when the proportion of labeled data is insufficient and when the domain similarity is limited.

Acknowledgements

This work was supported in part by the National Natural Science Foundation of China (61973067).

References

- [1] E. J. Topol, High-performance medicine: the convergence of human and artificial intelligence, *Nature medicine* 25 (1) 44–56 year=2019, publisher=Nature Publishing Group.
- [2] J. Noble, D. Boukerroui, Ultrasound image segmentation: a survey, *IEEE Transactions on Medical Imaging* 25 (8) (2006) 987–1010. doi:10.1109/TMI.2006.877092.
- [3] R. J. Van Sloun, R. Cohen, Y. C. Eldar, Deep learning in ultrasound imaging, *Proceedings of the IEEE* 108 (1) (2019) 11–29.
- [4] J. Ma, L. Bao, Q. Lou, D. Kong, Transfer learning for automatic joint segmentation of thyroid and breast lesions from ultrasound images, *International journal of computer assisted radiology and surgery* 17 (2) (2022) 363–372.
- [5] R. Roy, S. Ghosh, A. Ghosh, Speckle de-noising of clinical ultrasound images based on fuzzy spel conformity in its adjacency, *Applied Soft Computing* 73 (2018) 394–417.
- [6] R. M. Haralick, L. G. Shapiro, Image segmentation techniques, *Computer vision, graphics, and image processing* 29 (1) (1985) 100–132.
- [7] Y. LeCun, Y. Bengio, G. Hinton, Deep learning, *nature* 521 (7553) (2015) 436–444.
- [8] G. Litjens, T. Kooi, B. E. Bejnordi, A. A. A. Setio, F. Ciompi, M. Ghafoorian, J. A. van der Laak, B. van Ginneken, C. I. Sánchez, A survey on deep learning in medical image analysis, *Medical Image Analysis* 42 (2017) 60–88. doi:<https://doi.org/10.1016/j.media.2017.07.005>.
URL <https://www.sciencedirect.com/science/article/pii/S1361841517301135>

- [9] Z. Long, X. Zhang, C. Li, J. Niu, X. Wu, Z. Li, Segmentation and classification of knee joint ultrasonic image via deep learning, *Applied Soft Computing* 97 (2020) 106765.
- [10] O. Ronneberger, P. Fischer, T. Brox, U-net: Convolutional networks for biomedical image segmentation, in: *International Conference on Medical image computing and computer-assisted intervention*, Springer, 2015, pp. 234–241.
- [11] Y. Guo, X. Duan, C. Wang, H. Guo, Segmentation and recognition of breast ultrasound images based on an expanded u-net, *Plos one* 16 (6) (2021) e0253202.
- [12] J. Yang, M. Faraji, A. Basu, Robust segmentation of arterial walls in intravascular ultrasound images using dual path u-net, *Ultrasonics* 96 (2019) 24–33.
- [13] H. Li, J. Li, X. Guan, B. Liang, Y. Lai, X. Luo, Research on overfitting of deep learning, in: *2019 15th International Conference on Computational Intelligence and Security (CIS)*, IEEE, 2019, pp. 78–81.
- [14] Y. Yang, J. Guo, Q. Ye, Y. Xia, P. Yang, A. Ullah, K. Muhammad, A weighted multi-feature transfer learning framework for intelligent medical decision making, *Applied Soft Computing* 105 (2021) 107242.
- [15] H.-C. Shin, H. R. Roth, M. Gao, L. Lu, Z. Xu, I. Nogues, J. Yao, D. Mollura, R. M. Summers, Deep convolutional neural networks for computer-aided detection: Cnn architectures, dataset characteristics and transfer learning, *IEEE Transactions on Medical Imaging* 35 (5) (2016) 1285–1298. doi: 10.1109/TMI.2016.2528162.
- [16] H.-C. Shin, H. R. Roth, M. Gao, L. Lu, Z. Xu, I. Nogues, J. Yao, D. Mollura, R. M. Summers, Deep convolutional neural networks for computer-aided detection: Cnn architectures, dataset characteristics and transfer learning, *IEEE transactions on medical imaging* 35 (5) (2016) 1285–1298.

- [17] W. Zhang, X. Li, H. Ma, Z. Luo, X. Li, Transfer learning using deep representation regularization in remaining useful life prediction across operating conditions, *Reliability Engineering & System Safety* 211 (2021) 107556.
- [18] Y. Ding, M. Jia, J. Zhuang, P. Ding, Deep imbalanced regression using cost-sensitive learning and deep feature transfer for bearing remaining useful life estimation, *Applied Soft Computing* 127 (2022) 109271.
- [19] S. Chen, H. Yao, F. Qiao, Y. Ma, Y. Wu, J. Lu, Vehicles driving behavior recognition based on transfer learning, *Expert Systems with Applications* 213 (2023) 119254.
- [20] D. Sisodia, D. S. Sisodia, Feature space transformation of user-clicks and deep transfer learning framework for fraudulent publisher detection in on-line advertising, *Applied Soft Computing* 125 (2022) 109142.
- [21] X. Wu, Y. Feng, S. Lou, H. Zheng, B. Hu, Z. Hong, J. Tan, Improving neucube spiking neural network for eeg-based pattern recognition using transfer learning, *Neurocomputing* 529 (2023) 222–235.
- [22] M. H. Yap, G. Pons, J. Martí, S. Ganau, M. Sentis, R. Zwiggelaar, A. K. Davison, R. Marti, Automated breast ultrasound lesions detection using convolutional neural networks, *IEEE journal of biomedical and health informatics* 22 (4) (2017) 1218–1226.
- [23] G. Ayana, K. Dese, S.-w. Choe, Transfer learning in breast cancer diagnoses via ultrasound imaging, *Cancers* 13 (4) (2021) 738.
- [24] F. M. Calisto, N. Nunes, J. C. Nascimento, Breast screening: On the use of multi-modality in medical imaging diagnosis, in: *Proceedings of the International Conference on Advanced Visual Interfaces*, 2020, pp. 1–5.
- [25] Y. Song, J. Zheng, L. Lei, Z. Ni, B. Zhao, Y. Hu, Ct2us: Cross-modal transfer learning for kidney segmentation in ultrasound images with synthesized data, *Ultrasonics* (2022) 106706.

- [26] Z. Zhang, Z. Ji, Q. Chen, S. Yuan, W. Fan, Joint optimization of cyclegan and cnn classifier for detection and localization of retinal pathologies on color fundus photographs, *IEEE Journal of Biomedical and Health Informatics* 26 (1) (2021) 115–126.
- [27] J. P. Kieselmann, C. D. Fuller, O. J. Gurney-Champion, U. Oelfke, Cross-modality deep learning: Contouring of mri data from annotated ct data only, *Medical physics* 48 (4) (2021) 1673–1684.
- [28] H. Huang, H. Chen, H. Xu, Y. Chen, Q. Yu, Y. Cai, Q. Zhang, Cross-tissue/organ transfer learning for the segmentation of ultrasound images using deep residual u-net, *Journal of Medical and Biological Engineering* 41 (2) (2021) 137–145.
- [29] W. Zhang, L. Deng, D. Wu, Overcoming negative transfer: A survey, *arXiv preprint arXiv:2009.00909* (2020) 36.
- [30] X. Ying, Y. Zhang, X. Wei, M. Yu, J. Zhu, J. Gao, Z. Liu, X. Li, R. Yu, Msdan: Multi-scale self-attention unsupervised domain adaptation network for thyroid ultrasound images, in: 2020 IEEE International Conference on Bioinformatics and Biomedicine (BIBM), IEEE Computer Society, Los Alamitos, CA, USA, 2020, pp. 871–876. doi:10.1109/BIBM49941.2020.9313202.
URL <https://doi.ieeecomputersociety.org/10.1109/BIBM49941.2020.9313202>
- [31] Y. Jiang, N. Tan, T. Peng, Optic disc and cup segmentation based on deep convolutional generative adversarial networks, *IEEE Access* 7 (2019) 64483–64493. doi:10.1109/ACCESS.2019.2917508.
- [32] Y. Ganin, V. Lempitsky, Unsupervised domain adaptation by backpropagation, in: International conference on machine learning, PMLR, 2015, pp. 1180–1189.

- [33] Y. Ganin, E. Ustinova, H. Ajakan, P. Germain, H. Larochelle, F. Laviolette, M. Marchand, V. Lempitsky, Domain-Adversarial Training of Neural Networks, *JOURNAL OF MACHINE LEARNING RESEARCH* 17 (2016).
- [34] X. Li, Y. Xu, N. Li, B. Yang, Y. Lei, Remaining useful life prediction with partial sensor malfunctions using deep adversarial networks, *IEEE/CAA Journal of Automatica Sinica* 10 (1) (2022) 121–134.
- [35] S. Jin, L. Chen, R. Sun, S. McLoone, A novel vslam framework with unsupervised semantic segmentation based on adversarial transfer learning, *Applied Soft Computing* 90 (2020) 106153.
- [36] T. Han, C. Liu, R. Wu, D. Jiang, Deep transfer learning with limited data for machinery fault diagnosis, *Applied Soft Computing* 103 (2021) 107150.
- [37] X. Liao, Y. Qian, Y. Chen, X. Xiong, Q. Wang, P.-A. Heng, Mmtlnet: Multi-modality transfer learning network with adversarial training for 3d whole heart segmentation, *Computerized Medical Imaging and Graphics* 85 (2020) 101785.
- [38] P. Liu, C. T. Tran, B. Kong, R. Fang, Cada: Multi-scale collaborative adversarial domain adaptation for unsupervised optic disc and cup segmentation, *Neurocomputing* 469 (2022) 209–220.
- [39] J. Peng, J. Yi, Z. Yuan, Unsupervised mitochondria segmentation in em images via domain adaptive multi-task learning, *IEEE Journal of Selected Topics in Signal Processing* 14 (6) (2020) 1199–1209.
- [40] J. Wang, W. Li, Y. Chen, W. Fang, W. Kong, Y. He, G. Shi, Weakly supervised anomaly segmentation in retinal oct images using an adversarial learning approach, *Biomedical optics express* 12 (8) (2021) 4713–4729.
- [41] J. Hong, S. C.-H. Yu, W. Chen, Unsupervised domain adaptation for cross-modality liver segmentation via joint adversarial learning and self-learning, *Applied Soft Computing* 121 (2022) 108729.

- [42] M. De Bois, M. A. El Yacoubi, M. Ammi, Adversarial multi-source transfer learning in healthcare: Application to glucose prediction for diabetic people, *Computer Methods and Programs in Biomedicine* 199 (2021) 105874.
- [43] Y. Mansour, M. Mohri, A. Rostamizadeh, Domain adaptation with multiple sources, *Advances in neural information processing systems* 21 (2008).
- [44] B. Yang, S. Xu, Y. Lei, C.-G. Lee, E. Stewart, C. Roberts, Multi-source transfer learning network to complement knowledge for intelligent diagnosis of machines with unseen faults, *Mechanical Systems and Signal Processing* 162 (2022) 108095.
- [45] Q. Gu, Q. Dai, H. Yu, R. Ye, Integrating multi-source transfer learning, active learning and metric learning paradigms for time series prediction, *Applied Soft Computing* 109 (2021) 107583.
- [46] J. Bai, J. Jia, L. F. Capretz, A three-stage transfer learning framework for multi-source cross-project software defect prediction, *Information and Software Technology* 150 (2022) 106985.
- [47] L. Ge, J. Gao, H. Ngo, K. Li, A. Zhang, On handling negative transfer and imbalanced distributions in multiple source transfer learning, *Statistical Analysis and Data Mining: The ASA Data Science Journal* 7 (4) (2014) 254–271.
- [48] J. Tian, D. Han, M. Li, P. Shi, A multi-source information transfer learning method with subdomain adaptation for cross-domain fault diagnosis, *Knowledge-Based Systems* 243 (2022) 108466.
- [49] W. Zhouzhi, Z. Xiaomin, Z. Zhipeng, Z. Hengjia, T. Hongwu, Multi-source sintering transfer learning in small dataset sintering prediction scenario, *International Journal of Material Forming* 14 (5) (2021) 1157–1170.
- [50] J. Li, W. Wu, D. Xue, P. Gao, Multi-source deep transfer neural network algorithm, *Sensors* 19 (18) (2019) 3992.

- [51] W. Wu, Multi-source selection transfer learning with privacy-preserving, *Neural Processing Letters* 54 (6) (2022) 4921–4950.
- [52] X. Li, H. Jiang, M. Xie, T. Wang, R. Wang, Z. Wu, A reinforcement ensemble deep transfer learning network for rolling bearing fault diagnosis with multi-source domains, *Advanced Engineering Informatics* 51 (2022) 101480.
- [53] Q. She, Y. Cai, S. Du, Y. Chen, Multi-source manifold feature transfer learning with domain selection for brain-computer interfaces, *Neurocomputing* 514 (2022) 313–327.
- [54] Z. Luo, X. Zhang, S. Lu, S. Yi, Domain consistency regularization for unsupervised multi-source domain adaptive classification, *Pattern Recognition* 132 (2022) 108955.
- [55] X. Fang, G. Gong, G. Li, L. Chun, P. Peng, W. Li, A general multi-source ensemble transfer learning framework integrate of lstm-dann and similarity metric for building energy prediction, *Energy and Buildings* 252 (2021) 111435.
- [56] K. Li, J. Lu, H. Zuo, G. Zhang, Dynamic classifier alignment for unsupervised multi-source domain adaptation, *IEEE Transactions on Knowledge and Data Engineering* (2022).
- [57] J. Dong, Z. Fang, A. Liu, G. Sun, T. Liu, Confident anchor-induced multi-source free domain adaptation, *Advances in Neural Information Processing Systems* 34 (2021) 2848–2860.
- [58] H. Zhang, L. Guo, D. Wang, J. Wang, L. Bao, S. Ying, H. Xu, J. Shi, Multi-source transfer learning via multi-kernel support vector machine plus for b-mode ultrasound-based computer-aided diagnosis of liver cancers, *IEEE Journal of Biomedical and Health Informatics* 25 (10) (2021) 3874–3885.
- [59] I. Goodfellow, J. Pouget-Abadie, M. Mirza, B. Xu, D. Warde-Farley, S. Ozair, A. Courville, Y. Bengio, Generative adversarial nets, in:

- Z. Ghahramani, M. Welling, C. Cortes, N. Lawrence, K. Q. Weinberger (Eds.), *Advances in Neural Information Processing Systems*, Vol. 27, Curran Associates, Inc., 2014.
URL <https://proceedings.neurips.cc/paper/2014/file/5ca3e9b122f61f8f06494c97b1afccf3-Paper.pdf>
- [60] T. Zhou, S. Ruan, S. Canu, A review: Deep learning for medical image segmentation using multi-modality fusion, *Array* 3 (2019) 100004.
- [61] K. He, X. Zhang, S. Ren, J. Sun, Deep residual learning for image recognition, in: *Proceedings of the IEEE conference on computer vision and pattern recognition*, 2016, pp. 770–778.
- [62] T. Yang, X. Yu, N. Ma, Y. Zhao, H. Li, A novel domain adaptive deep recurrent network for multivariate time series prediction, *Engineering Applications of Artificial Intelligence* 106 (2021) 104498.
doi:<https://doi.org/10.1016/j.engappai.2021.104498>.
URL <https://www.sciencedirect.com/science/article/pii/S0952197621003468>
- [63] W. Al-Dhabyani, M. Gomaa, H. Khaled, A. Fahmy, Dataset of breast ultrasound images, *Data in brief* 28 (2020) 104863.
- [64] L. Pedraza, C. Vargas, F. Narváez, O. Durán, E. Muñoz, E. Romero, An open access thyroid ultrasound image database, in: *10th International Symposium on Medical Information Processing and Analysis*, Vol. 9287, International Society for Optics and Photonics, 2015, p. 92870W.
- [65] Q. Zhou, Q. Wang, Y. Bao, L. Kong, X. Jin, W. Ou, Laednet: A lightweight attention encoder–decoder network for ultrasound medical image segmentation, *Computers & Electrical Engineering* 99 (2022) 107777.
- [66] H. Zou, X. Gong, J. Luo, T. Li, A robust breast ultrasound segmentation method under noisy annotations, *Computer Methods and Programs in Biomedicine* 209 (2021) 106327.

- [67] J. Ding, Z. Huang, M. Shi, C. Ning, Automatic thyroid ultrasound image segmentation based on u-shaped network, in: 2019 12th International Congress on Image and Signal Processing, BioMedical Engineering and Informatics (CISP-BMEI), IEEE, 2019, pp. 1–5.
- [68] D. Koundal, S. Gupta, S. Singh, Computer aided thyroid nodule detection system using medical ultrasound images, Biomedical Signal Processing and Control 40 (2018) 117–130.
- [69] Y. Wu, K. He, Group normalization, in: Proceedings of the European conference on computer vision (ECCV), 2018, pp. 3–19.